Sedimentologika

Research article

Contrasting sedimentary and long-lasting geochemical imprints of seismic shaking in a small, groundwater-fed lake basin (Klopeiner See, Eastern European Alps)

Christoph Daxer[1], Katleen Wils[1,2], Arne Ramisch[1], Michael Strasser[1], Jasper Moernaut[1*]

[1] Sedimentary Geology Research Group, Institute of Geology, University of Innsbruck (Austria)
[2] Renard Centre of Marine Geology, Department of Geology, Ghent University (Belgium)

*corresponding authors: Jasper Moernaut (Jasper.Moernaut@uibk.ac.at)

doi: 10.57035/journals/sdk.2024.e21.1296

Editors: Suzanne Bull and Katrina Kremer
Reviewers: Renaldo Gastineau and one anonymous reviewer
Copyediting, layout and production: Romain Vaucher, Liz Mahon and Sophie Hage

Submitted: 30.10.2023
Accepted: 19.03.2024
Published: 06.05.2024

Abstract | In slowly deforming tectonic settings (e.g., European Alps), large earthquakes occur too infrequently to be adequately represented in instrumental and historical records. This leads to uncertainties and inaccuracies of seismic hazard estimations. To extend the seismic record, lacustrine paleoseismologists usually resort to the sedimentary archive of large lakes where earthquakes can be recorded as mass-transport deposits and associated turbidites. The imprint of seismic shaking is generally more subtle and poorly understood in small lakes (<2 km^2) with small catchments and therefore such sediment-starved basins are often neglected for paleoseismology. However, these basins might harbour additional information about past earthquakes, thus constituting a valuable supplement to other paleoseismic data. Here, we present the 18 ka-long paleoseismic record of Klopeiner See, a small and rather shallow groundwater-fed lake in the Eastern European Alps. Reflection seismic profiles and sediment cores reveal that several large earthquakes led to extensive mass-wasting in early Late-Glacial times when sedimentation rates were very high (~10 mm/yr). In the Early and Middle Holocene, low sedimentation rates (~0.2-0.5 mm/yr) may have decreased the lake's sensitivity for recording seismic shaking and no imprints were found for paleo-earthquakes inferred from other records in the region. A short succession of turbidites at ca. 3160 cal BP suggests a burst of strong paleoseismic activity. This may have caused permanent modifications of inflowing ground water systems, archived as a permanent shift in the geochemical signal of the sediment. Such a period of enhanced paleoseismic activity was also inferred from the nearby Lake Wörthersee, but it remains unclear whether these represent the same earthquakes or migrating paleoseismicity. This study highlights the unexpected potential and peculiarities of paleoseismology on small ground-water fed lakes.

Lay summary | This study examines the sediments of Klopeiner See, a small (1.1 km^2) ground-water fed lake in the Eastern European Alps. It aims to investigate the occurrence of earthquakes close to the lake in the last 18000 years. A detailed seismic-reflection survey and long (~14.5 m) sediment cores reveal multiple large underwater landslides that were triggered by large earthquakes in the Late Glacial (at around 16000 years before present). A sequence of smaller deposits of underwater mud avalanches reveals that several earthquakes occurred in short succession around 3160 years ago. These earthquakes probably caused changes in the groundwater system that feeds Klopeiner See, as indicated by large permanent changes in the geochemistry of the sediment cores. This is a phenomenon seldom described in literature so far. Our study thus highlights the importance of the investigation of small lakes to improve our knowledge of the timing of past earthquakes, and the impacts associated with earthquakes on the natural environment.

Keywords: Earthquake, Lake sediment, Paleoseismicity, Eastern Alps, Sediment geochemistry

1. Introduction

Areas with low tectonic deformation rates (<5 mm/yr) typically show minor to moderate seismicity and large damaging earthquakes are rather rare. Interseismic times between large events often exceed the time span of instrumental seismicity or historical records (Stein & Liu, 2009). In contrast to the seismic cycle of great earthquakes at active plate boundaries, earthquakes in slow-deformation settings typically show episodic, clustered, and spatially migrating occurrence (Landgraf et al., 2017). It therefore remains unclear whether current seismic hazard assessments for slow-deformation settings adequately capture the occurrence probability and damage potential of such extreme events.

Lake paleoseismology can provide invaluable information on the occurrence and strength of past seismic shaking. Such information enables (1) establishing earthquake recurrence patterns (Moernaut, 2020), (2) constraining the maximum credible earthquake (MCE) and associated distribution of seismic intensity and damage potential (Oswald et al., 2022), and (3) testing of seismic hazard maps (Daxer et al., 2022a). These studies are usually carried out on relatively large and deep lake systems, in which strong seismic shaking triggers the failure of subaqueous sedimentary slopes and delta fans, leading to the deposition of mass-transport deposits (MTDs) and associated turbidites on the basin plains (Moernaut et al., 2007; Praet et al., 2017; Schnellmann et al., 2002). In contrast, lake paleoseismology studies on small (<2 km^2 surface area), relatively shallow (<50 m depth) and isolated basins are relatively scarce because sedimentary imprints of seismic shaking can be absent or rather subtle. These imprints include seiche deposits (Avşar et al., 2014), geochemical changes (Archer et al., 2019), turbidites from delta failure (Van Daele et al., 2019), soft-sediment deformation structures (Monecke et al., 2006) and fractured sediments (Becker et al., 2002). Moreover, small lakes in formerly glaciated regions often exhibit a dramatic switch in sediment dynamics from rapid, clastic sedimentation fed by glacial meltwater streams towards slow, organic-rich sedimentation in isolated water bodies (Fritz et al., 2012; Ojala et al., 2019; Roberts et al., 2022). Such drastic changes in sedimentation type and rate may significantly affect the sensitivity of lake systems to seismic shaking and thus their paleoseismic potential (Rapuc et al., 2018), but quantitative constraints on this are lacking. In contrast to large and deep lakes, smaller lakes are plentiful in many regions worldwide, allowing for a significant increase in the number of sites for regional paleoseismic studies. Such regional studies allow the location and magnitude of paleo-earthquakes to be reconstructed, which is key information for seismic hazard evaluations (Howarth et al., 2021; Kremer et al., 2017; Strasser et al., 2006; Vanneste et al., 2018; Wils et al., 2020). Therefore, it is vital to advance our understanding of how sedimentary sequences in small lake systems can register strong earthquake shaking so that we can fully exploit their paleoseismic potential.

In this study, we present the 18 ka long sedimentary record of a small groundwater-fed lake (Klopeiner See) in the slowly-deforming European Eastern Alps, in which we identify and discuss different types of sedimentary and geochemical imprints related to historical and prehistorical earthquake shaking.

2. Study area

2.1. Seismotectonic setting

Klopeiner See (*See* = German for lake; 46°36'15"N, 14°35'02"E) is situated in the Austrian federal state of Carinthia, just north of the Periadriatic fault (Figure 1A, B). Here, the seismotectonic regime is controlled by the northward indentation and anticlockwise rotation of the Adriatic microplate in relation to the European plate and the Pannonian fragment (Figure 1A). This process has been active since the late Oligocene/Middle Miocene and currently leads to plate convergence of ~2-3 mm/yr (Sánchez et al., 2018) and ongoing eastward extrusion of decoupled crustal blocks along low angle normal faults and major strike-slip fault systems (Ratschbacher et al., 1991) that border the study area. The most important fault systems are all right-lateral and include: the Periadriatic fault system (including the Sava and Šoštanj faults) in the south, separating the Eastern Alps from the Southern Alps (Kastelic et al., 2008); the Mölltal fault in the west; and the Lavanttal fault in the east (Figure 1B). Along these fault systems, moderate to strong earthquakes (M>5) with damage potential are scarce. Minor earthquakes, however, are frequent, indicating that the lateral extrusion is an ongoing process (Figure 1B; Eder & Neubauer, 2000; Reinecker & Lenhardt, 1999). Seismicity is widespread (diffuse) and many earthquake locations cannot be linked to the main fault systems (Figure 1B), but may relate to the many "suspected" faults that are presented on the geological maps (Figure 1C). Near Klopeiner See, these "suspected" faults are based on topographic lineaments and a few field observations (Stiny, 1934) but their existence is questionable.

2.2. Historical seismicity and paleoseismology

Due to the aforementioned fault systems and its position close to the seismically active areas in Friuli (Italy) and western Slovenia, Carinthia is among the regions with the highest seismic hazard in Austria (Weginger et al., 2019). Over the last ~800 years, the region around Klopeiner See has experienced several earthquakes of local intensities (I_L) > V on the European Macroseismic scale (EMS-98) (Grünthal et al., 2013; Rovida et al., 2022; Stucchi et al., 2013): in 1976 CE (M_w 6.4; I_L V-V½), 1899 CE (M_w ~4.9; I_L VI-VII), 1895 CE (M_w ~6; I_L V-VI), 1857 CE (M_w ~5.1; I_L ~V½), 1690 CE (M_w ~6.2-6.5; I_L VI-VII), 1511 CE (M_w ~6.3-6.9; I_L V½) and 1348 CE (M_w ~6.6-7; I_L VI½-VII). The latter presumably constitutes the largest documented historical earthquake in the Alps, caused major rockslides at the Dobratsch Mountain (Figure 1B) and remobilized large

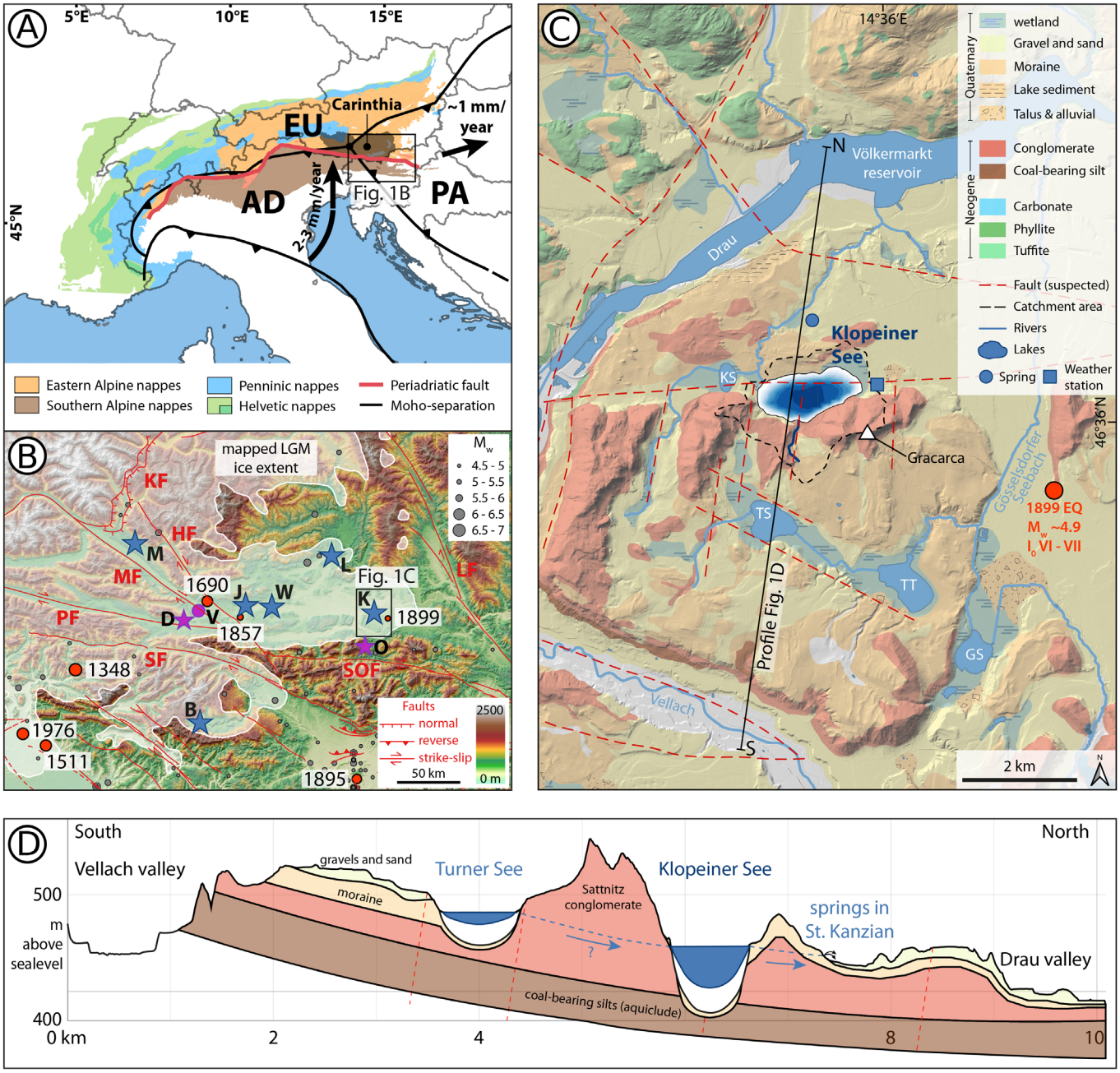

Figure 1 | Overview of the study area. (A) Simplified tectonic map (simplified after Schmid et al., 2004) and crustal architecture of the European Alps (modified after Brückl et al., 2010 and Faccenna et al., 2004). The counterclockwise rotation of the Adriatic plate (AD) relative to the European plate (EU) causes the eastward motion of the Pannonian fragment (PA). (B) Local topography and historical and instrumental seismicity (> M_w 4.5) of the study area. Earthquake data from the Austrian Earthquake Catalogue, AEC (ZAMG, 2021) and the European Pre-instrumental Earthquake Catalogue (EPICA; Rovida et al., 2022). Important earthquakes for this study are marked in red. The red lines denote important active or probably active faults compiled from Atanackov et al., 2021 and Schmid et al., 2004: HF – Hochstuhl fault, KF – Katschberg fault, LF – Lavanttal fault, MF – Mölltal fault, PF – Periadriatic fault, SOF – Šoštanj fault, SF – Sava fault. Blue stars denote lakes mentioned in the manuscript: B – Lake Bohinj, J – Jeserzer See, K – Klopeiner See, L – Längsee, M – Millstätter See, W – Wörthersee. The purple stars indicate the Dobratsch mountain (D) and Obir cave (O), the purple dot marks the town of Villach (V). The whitened area marks the mapped LGM ice extent (after van Husen, 1987, 2011). (C) Geologic map of the surroundings of Klopeiner See (after Kahler, 1962; Moser, 2020; and Stiny, 1934). The blue dot north of Klopeiner See marks springs that are fed by water from Klopeiner See (Messiner & Windisch, 2008). GS – Gösselsdorfer See, KS – Kleinsee, TS – Turnersee, TT – Tomerteich. (D) Simplified cross–section through Turnersee and Klopeiner See. The lakes are underlain by Miocene silts that act as an aquiclude and dip to the north. The Sattnitz conglomerate, on the other hand, is permeable.

sediment volumes on the bottom of Millstätter See and Wörthersee (Daxer et al., 2022b). The sedimentary imprint (i.e., number and volume of mass transport deposits, extent and cumulative thickness of turbidites) of the other strongest historical earthquakes is either modest (e.g., 1511 CE, 1690 CE, 1857 CE) or potentially absent (e.g., 1976 CE) in these lakes and overall scales to the local seismic intensities. Based on this calibration applied to several long cores in the different basins of Wörthersee, a 14 ka-long quantified paleoseismic record was established that allowed the local seismic hazard curve to be tested (Daxer et al., 2022a). In the Julian Alps (Slovenia), a 6.6

ka long paleoseismic record was obtained from Lake Bohinj, which contains imprints of the historical 1348 CE, 1511 CE and 1690 CE earthquakes (Rapuc et al., 2018). In the Eastern Southern Alps (Friuly), the sediments of Cavazzo Lake recorded the nearby 1976 CE earthquake and related shocks in 1976-1977 CE (Polonia et al., 2021), but the cores do not go back far enough in time to study other historical earthquakes. More relevant for our study area is the Obir cave (Baroň et al., 2022), which is located only 11 km south of Klopeiner See. Three events occurred in Obir Cave: Here, dm-scale fault slip ca. 41.8–18.7 ka ago, cm-scale fault slip occurred ca. 10.7–8.6 ka ago, and a speleothem damage event occurred ca. 6.3–5.7 ka ago. These are interpreted as the result of destructive to very destructive paleo-earthquakes with local intensity of VIII-X on the ESI-2007 scale.

2.3. Glacial evolution and hydrogeology of Klopeiner See

Klopeiner See is located ~13 km west (i.e., inside) of the mapped Last Glacial Maximum (LGM) ice extent (Figure 1B; van Husen, 2011), which was reached ca. 27000-21000 cal BP in the south-eastern Alps (Monegato et al., 2007). Alpine glaciers decayed rapidly after the onset of deglaciation, as indicated by radiocarbon dating of peat bogs in inneralpine valleys, e.g., the central Inn valley was ice-free at ~17400 cal BP (Bortenschlager, 1984) and the basin of Bad Mitterndorf was ice-free as early as ~18700 cal BP (Draxler, 1977; Reitner, 2007). Radiocarbon dates from basal lake sediments in Längsee and Jeserzer See, located ~24 km northwest and ~40 km west of Klopeiner See (Figure 1B) respectively, indicate ice free conditions at ~19000 cal BP at Längsee (Huber et al., 2010; Schmidt et al., 1998) and at ~18500 cal BP at the more internal Jeserzer See (Schmidt et al., 2012). The onset of (glacio-) lacustrine sedimentation in Klopeiner See can thus be estimated to a minimum age of 18500 ± 500 cal BP.

Klopeiner See is located at the northern edge of the so-called "Rückersdorfer-Platte", a plateau bordered by the rivers Drau, Vellach, and Gösselsdorfer Seebach (Figure 1C). This plateau mainly consists of permeable conglomerates ("Sattnitz-conglomerate") that were deposited in the Klagenfurt intra-orogenic basin during the Neogene (Nemes et al., 1997; Stiny, 1934). These conglomerates are underlain by clayey, coal bearing units, which form the aquiclude of the Rückersdorfer Plateau (Messiner & Windisch, 2008). The Sattnitz-conglomerate forms the hills along the southern shore of Klopeiner See (i.e., the highest point called the "Gracarca" at an elevation of 676 m; Figure 1C), while the northern shore mainly consists of permeable Quaternary conglomerates and moraines that overlie the Sattnitz-conglomerate.

The lake lies at an altitude of 446 m above sea level, is ~48 m deep and has a relatively small catchment size of about 2.4-4.1 km^2 (according to different sources; Borasi et al., 2013; Kärntner Institut für Seenforschung, 2021) compared to its surface area of 1.1 km^2. The lake consists of a single basin. There are no perennial rivers draining the catchment (Borasi et al., 2013). On the southern and south-eastern shore, four creeks enter the lake, but the discharge is mostly lower than 1 l/s (Messiner & Windisch, 2008). Most of the inflow (85%) results from groundwater flow through the Neogene conglomerates (Borasi et al., 2013). Together with its wind-protected position, this leads to a rapid warming of the water in spring and an important contribution of evaporation to its water balance. It has meromictic conditions (Reichmann et al., 2014), in which mixing of the water column is limited to the uppermost 30 m and the lake bottom water remains oxygen-free (Kärntner Institut für Seenforschung, 2021).

3. Methods

3.1. Seismic reflection surveys and mapping of mass-transport deposits

High-resolution reflection seismic data was acquired during two surveys in 2017 and 2018, using a single-channel 3.5 kHz Kongsberg Geopulse pinger (theoretical vertical resolution ~10 cm). Positioning was carried out with stand-alone GPS (see Figure 2A for traces of seismic profiles). Typical survey line spacing is 50 m and some circular lines at the base-of-slope were added for a better mapping of MTDs. The data were processed in the IHS Markit Kingdom Suite (v. 2021) software, applying a bandpass filter (2-6 kHz). The polarity of the seismic data follows the American standard: a reflection caused by an increase in acoustic impedance is considered a positive polarity and displayed as a peak (in blue colour). No phase shift was applied (zero phase). Sedimentary bodies with basin-ward thinning geometries, irregular top and/or bottom surface, and chaotic or heterogeneous seismic facies were identified as MTDs. Their seismic appearance differs strongly from regular background sedimentation, which is characterized by continuous reflections (Sammartini et al., 2019). Time-to-depth conversion was carried out using a constant acoustic velocity of 1500 m/s for both sediment and water. In figures showing seismic profiles, two-way travel time (TWT) of the seismic wave in milliseconds (ms) is given as a measure of depth as well. The bathymetric map of Klopeiner See (Figure 2A) was produced by tracking the lake floor and interpolating between the tracks and towards the outline of the lake. This was done in the software Surfer 10 (Golden Software), using the simple kriging interpolation algorithm. Similarly, thickness grids and the volumes of MTDs were calculated. For this, the bottom and top of the MTDs were used as the lower and upper boundaries. Areas where no data (i.e., no MTD) is available were cut from the grid. Depending on the area covered by MTDs, the grid spacing varied from 0.7 m to 10 m.

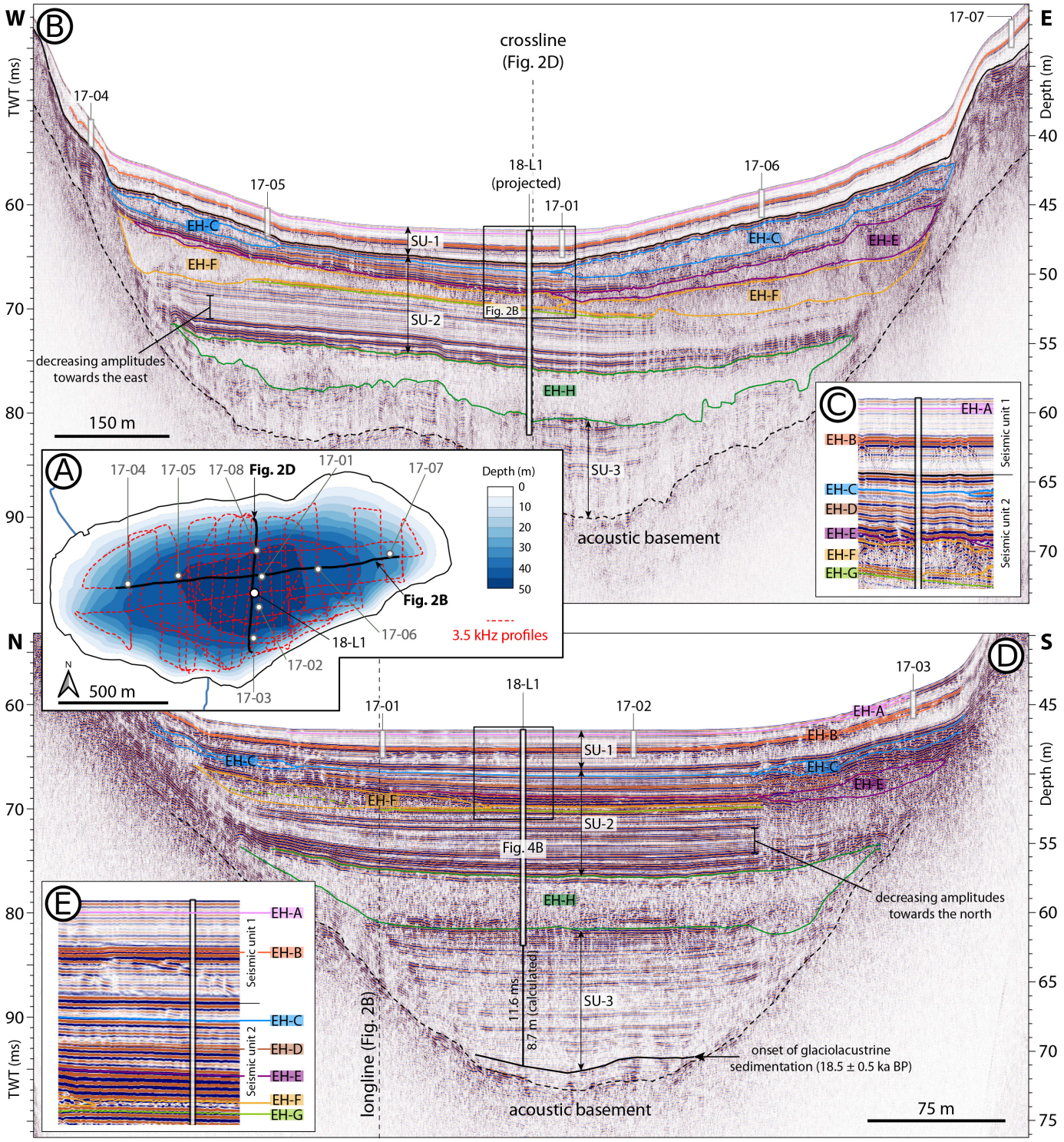

Figure 2 | Survey overview and seismic profiles of Klopeiner See. See Supplementary Figures 2 and 3 for uninterpreted seismic profiles. (A) Bathymetric map of Klopeiner See (based on seismic data) and overview of acquired seismic profiles and sediment cores. (B) Seismic profile along the main lake axis. The glaciolacustrine infill of Klopeiner See is divided into three seismic units (SUs). Coeval mass-transport deposits are marked in the same colour and assigned to an event-stratigraphic horizon (EH). The core location of long core KLOP18-L1 does not lie directly on the profile but is projected. (C) Detail of Figure 2B highlighting the event-stratigraphic horizons in the uppermost ~8 ms of the sedimentary infill. (D) Seismic profile perpendicular to the main lake axis. (E) Detail of Figure 2D highlighting the event-stratigraphic horizons in the uppermost ~8 ms of the sedimentary infill.

3.2. Sediment coring and sedimentological analyses

Short (ca. 1.5 m) sediment cores were retrieved in 2017 CE and 2018 CE using a gravity corer with a manual percussion system. In 2018 CE, a 14.58 m long, 6.3 cm diameter composite sediment core was acquired using the UWITEC percussion piston coring system of ETH Zürich (KLOP18-L1; 468168 E, 5161215 N, UTM 33N). The composite sediment core consists of three parallel cores (KLOP18-L1A, KLOP18-L1B and KLOP18-L1C; the latter only covering the depths of ~11.5-14.5 m) with overlapping 3 m sections that were cut into 1.5 m pieces. Due to an incomplete recovery, short core KLOP17-01 is used for the uppermost part of the composite core section of KLOP18-L1 (Supplementary Figure 1). X-ray computed tomography (CT) scanning was carried out on whole or

split sediment cores at the Medical University of Innsbruck, using a Siemens SOMATOM Definition A (voxel size = 0.2 x 0.2 x 0.3 mm). For visualization of the CT data, FIJI (Schindelin et al., 2012) was used. Magnetic susceptibility (MS) and γ-density were measured at 0.2 cm and 0.5 cm vertical resolution, respectively, using a GEOTEK Multi-Sensor Core Logger (MSCL) and a Bartington MS2E point sensor. High-resolution (0.2 mm step-size) X-ray fluorescence (XRF) scanning was carried out with an ITRAX core scanner at the Austrian Core Facility for scientific core logging and scanning (Institute of Geology, Innsbruck) using a Mo-tube (30 kV and 43 mA, exposure time 5 s). Statistical analysis of the XRF data (principal component analysis and Ward's hierarchical clustering; Ward, 1963) was carried out using the centred-log ratio corrected element counts (e.g., Weltje et al., 2015) of Si, K, Ca, Ti, Mn, Fe as well as the incoherent and coherent scattering (Mo inc and Mo coh). The ratio between Mo inc and Mo coh is used as an indicator for organic content (Croudace & Rothwell, 2015). Core photographs were acquired with the ITRAX core scanner and a Smartcube camera image scanner. Grain size data was acquired from bulk sediment using a Malvern Mastersizer 3000, applying 30 seconds of ultrasonication at 40% strength, and statistically evaluated using GRADISTAT v. 9.1 (Blott & Pye, 2001). The description of grain size distributions follows the standard parameters defined by Folk & Ward (1957). Sedimentary facies were distinguished via macroscopic visual description and microscopic smear slide analysis (following Schnurrenberger et al., 2003). Colour values are given following Munsell (2010). Turbidites were identified based on their relatively coarse grain size and high density in comparison to the background sedimentation and their characteristic fining upward sequence.

3.3. Dating and age-depth models

Accelerator Mass Spectrometry (AMS) radiocarbon measurements were performed on terrestrial organic macro-remains (leaves and needles) at the Ion beam Physics Laboratory of ETH Zürich and calibrated using the IntCal20 calibration curve (Reimer et al., 2020). Due to insufficient terrestrial organic macro-remains, however, the lowermost (i.e., oldest) radiocarbon sample consists of undetermined, hand-picked organic matter. Age-depth models of cores KLOP17-01 (short core) and KLOP18-L1 were calculated using the R-package Bacon (v. 2.5.7; Blaauw & Christen, 2011). In the age-depth modelling of core KLOP17-01, event deposits >0.3 cm were classified as "slumps" and therefore treated as instantaneous events by Bacon. In the age-depth model of core KLOP18-L1, which also covers rapidly deposited Late Glacial clastic sediments (see section 4.2), a higher threshold of 5 cm was chosen to avoid cutting out background sedimentation.

Varve counting (e.g., Zolitschka et al., 2015) was carried out on the uppermost part of the sedimentary sequence, where finely-laminated sediment is present (see section 4.2.4). The counting was performed on thin sections using both plane- and cross-polarized light after determining subsections of typically 2-5 cm length, bordered by easily recognizable markers (e.g., thicker laminae, detrital layers). Potential varve disturbances were circumvented by integrating over the whole width of the thin section. Each subsection was counted at least 3 times, and the average of the counts was retained for the final age-depth-model. To give a measure of the precision of the varve chronology, the minimum and maximum counts are given as the relative counting errors.

3.4. Calculation of local seismic intensities of historical and instrumental earthquakes

The historical and instrumental earthquakes considered in this study to calibrate the paleoseismic record of Klopeiner See stem from a combination of four earthquake catalogues: (1) the SHARE European Earthquake Catalogue (SHEEC) 1000-1899 (Stucchi et al., 2013), (2) the European PreInstrumental Earthquake CAtalogue (EPICA) 1000-1899 (Rovida et al., 2022) which is an update of SHEEC, (3) the SHARE European Earthquake Catalogue (SHEEC) 1899-2006 (Grünthal et al., 2013), and (4) the Austrian Earthquake Catalogue (AEC; ZAMG, 2021). We derive local seismic intensities (I_L) at Klopeiner See by using the intensity prediction equations (IPEs) developed for the Swiss Alps (Fäh et al., 2011; "Alpine" formulas; see also Álvarez-Rubio & Fäh, 2009), which provides different formulas depending on the hypocentral depth (less or more than 7 km) and distance (less or more than 55 km). For events with unknown depths, we

Core ID	Laboratory ID	Composite core depth (cm)	Event-free composite core depth (cm)	Radiocarbon age (a BP)	Error (1 sigma)	95% calibrated age range	Material
KLOP17-01_32.5-35cm	ETH-88624	28.3	28.3	210	26	305-…	leaf
KLOP17-01_75.5-76.5cm	ETH-119061	70.5	70.5	2348	24	2461-2331	leaf fragments
KLOP17-01_85.5-86.5cm	ETH-85098	80.5	80.5	3001	24	3327-3076	twig, leaf fragments
KLOP17-01_92-93cm	ETH-119062	87	87	3361	24	3688-3492	leaf
KLOP17-01_128.5-129.5cm	ETH-85089	123.5	123.5	6463	26	7427-7323	leaf fragments
KLOP18-L1B_1-2.5m_100cm	ETH-96540	192.4	192.4	13568	109	16755-16025	Needles, bark, veg. indet. (see Supplementary Figure 5)
KLOP18-L1B_4-5.5m_37-42cm	ETH-96542	444	321.7	14138	122	17675-16816	handpicked bulk organic matter

Table 1 | Radiocarbon ages of Klopeiner See sediment cores.

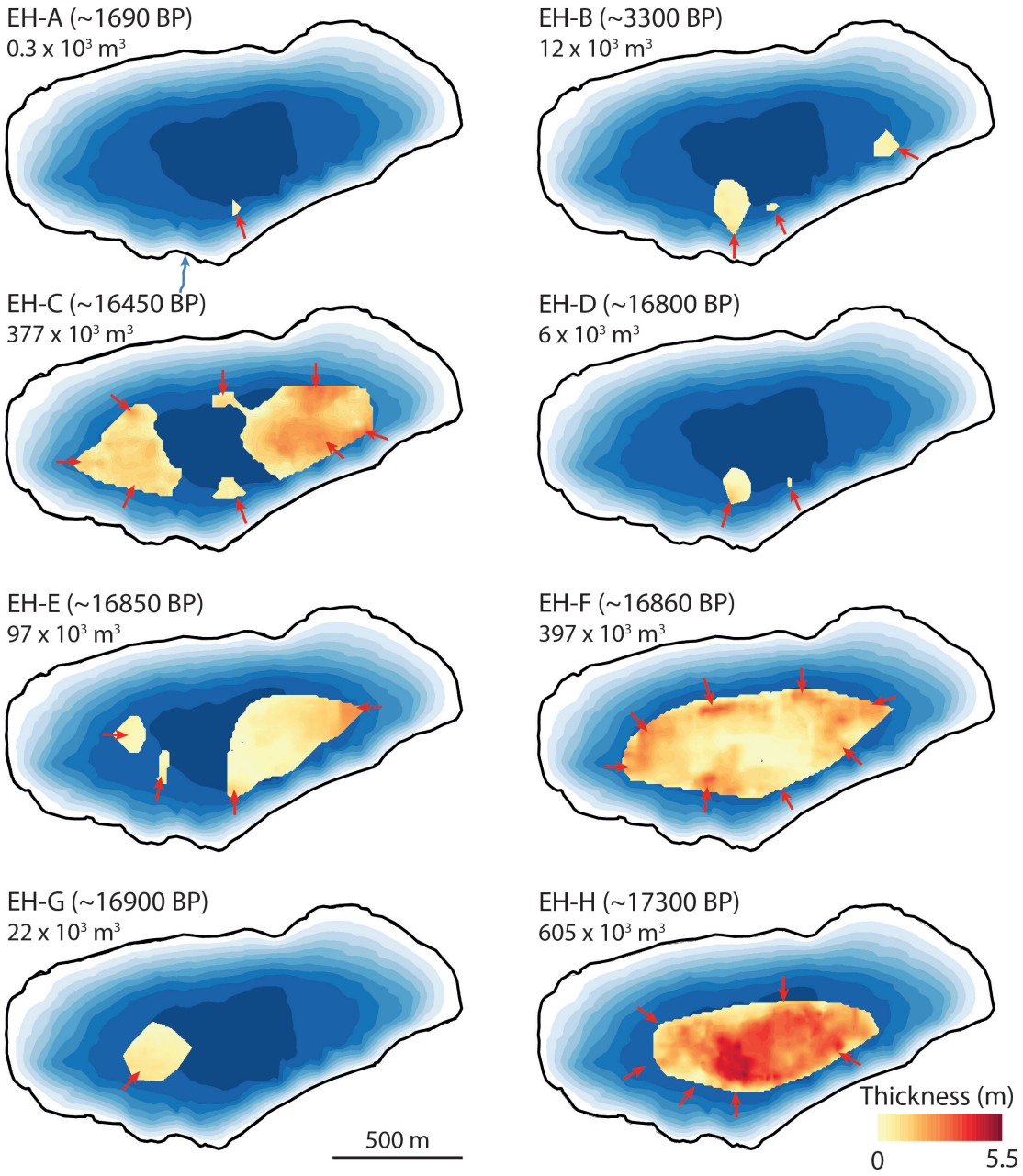

Figure 3 | Maps showing the thickness of MTDs attributed to the eight event-stratigraphic horizons of Klopeiner See. Red arrows denote the inferred source direction of individual MTDs.

consider that the event nucleated at the surface, which results in a maximum estimate for the shaking intensities at Klopeiner See. Errors of the calculated I_L result from uncertainties concerning the magnitude of the historical events, as given in the earthquake catalogues, rather than by considering the standard deviations given by the IPEs. To provide an additional idea of how uncertainties of magnitude and epicentral location influence our results, we calculated I_L based on both the SHEEC and EPICA catalogue and compared the results. This is especially relevant for the earthquakes of 1348, 1511 and 1690 for which the magnitude decreased by ~0.4, ~0.6 and ~0.3, respectively. The used data and the calculated local intensities are provided in Supplementary File 1.

4. Results

4.1. Seismic stratigraphy and mass-transport deposit event stratigraphy

The 3.5 kHz seismic data images the complete lacustrine infill of Klopeiner See, which comprises 35 ms (~26 m) of sediment maximum. The acoustic basement shows a chaotic, semi-transparent seismic facies and is capped by a high-amplitude, irregular reflection. Based on seismic facies characteristics, the sedimentary infill of Klopeiner See can be divided into three seismic units (SUs) within which there are several MTDs corresponding to one of eight event-stratigraphic horizons (EHs A-H) (Figure 2; see Supplementary Figures 2 & 3 for uninterpreted seismic profiles). SU-1 represents the uppermost ~4 ms of the stratigraphy. It is generally characterized by low amplitudes, except for a single high-amplitude reflection that divides

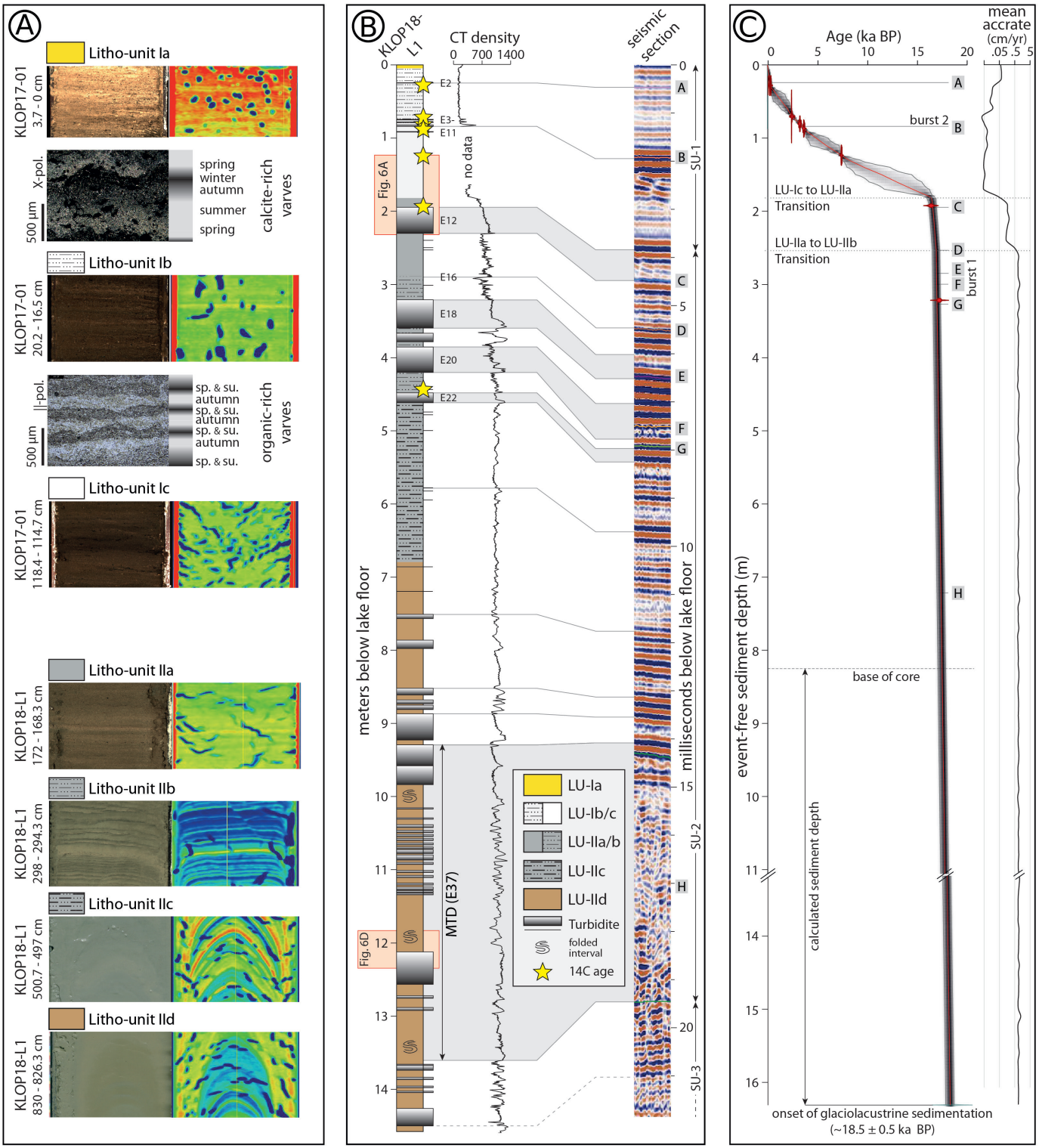

Figure 4 | Lithologies, core-to seismic correlation and age-depth model of core KLOP18-L1. (A) Based on macroscopic analysis, the sedimentary succession of core KLOP18-L1 is divided into seven lithological units (LUs), the uppermost two of which, LU-Ia and LU-Ib, show annual laminations (varves). (B) Core log and core-to-seismic correlation of core KLOP18-L1. Within the sedimentary succession, several turbidites and a large MTD are present. Together with lithological changes, they are responsible for variations in density, thus denoting important marker horizons for the core-to-seismic correlation. (C) Radiocarbon-based age-depth model and derived accumulation rates of core KLOP18-L1. The age-depth model was extended to the onset of glaciolacustrine sedimentation which is expected to be coeval with the post-LGM ice retreat and thus dates to 18500 ± 500 cal BP.

the SU-1 in two parts of similar thickness and is the origin of several reflection hyperbolas. In the lower part, the continuity of the reflections is frequently interrupted by hyperbolas originating from the single high-amplitude reflection. SU-1 forms a drape over the whole lake-floor topography. The underlying SU-2 is characterized by a ~10 ms thick ponding succession of laterally continuous reflections that in part converge from west to east and from south to north, coinciding with a decrease in reflection amplitude (Figure 2). It is separated from SU-3 by an up to 5 ms thick MTD (EH-H) covering the entire basin plain. In the main depocenter, SU-3 shows laterally continuous intermediate-amplitude reflections with varying spacing (Figure 2D). Near the acoustic basement, SU-3 shows

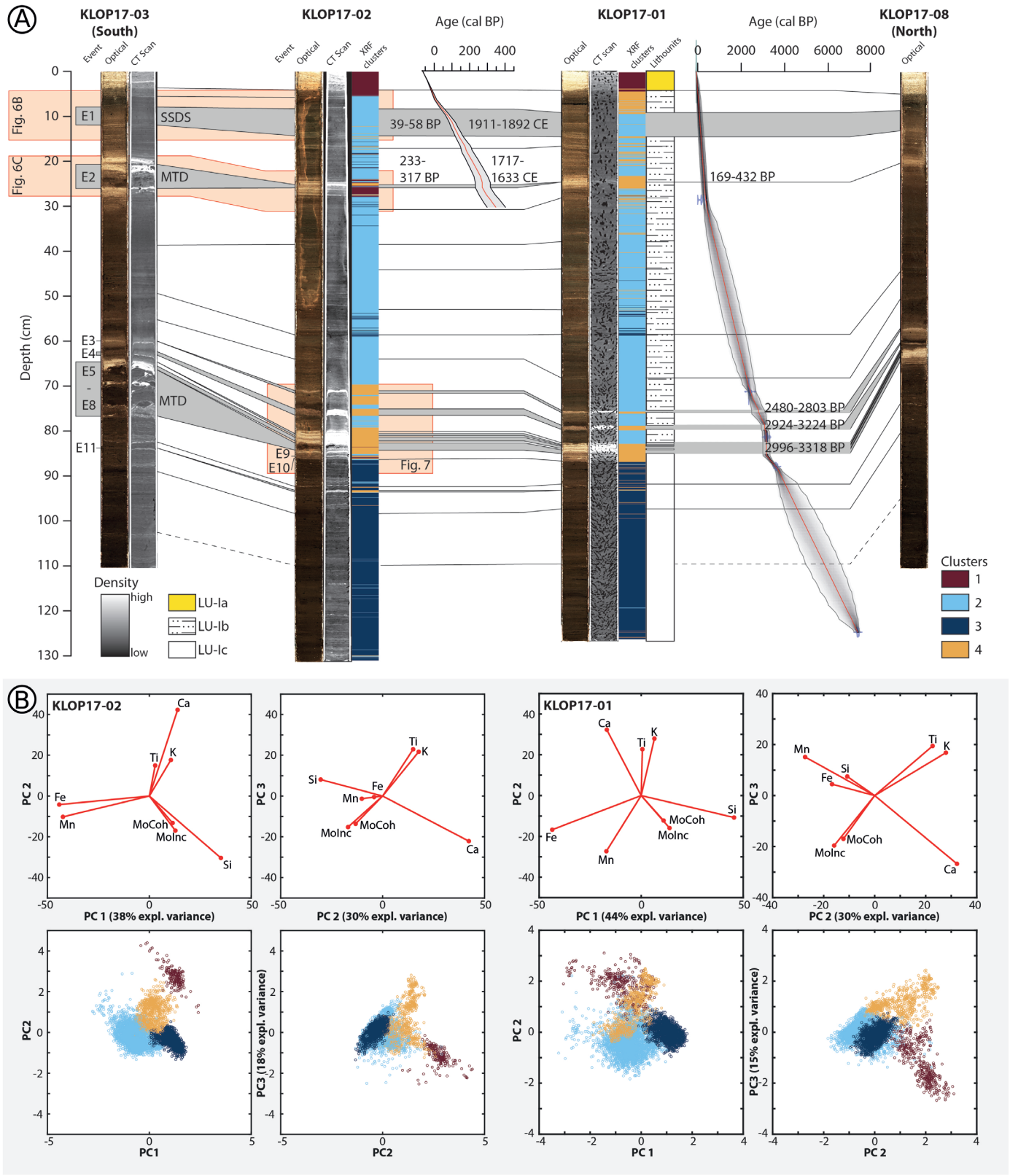

Figure 5 | Correlation of short cores and statistical analysis of XRF data. (A) Correlation of short cores along a south to north transect (see Figure 2A for core locations) and varve-based (KLOP17-02) and ^{14}C-based (KLOP17-01) age-depth models. Event layers are marked in grey. The clustering results of the XRF data are given as coloured bars. (B) PCA biplots. Individual measurements are coloured according to the clustering algorithm.

chaotic reflections of varying amplitude (Figure 2B). At the coring site of long core KLOP18-L1, the lower boundary of SU-3 lies at ~95 ms TWT (~71.25 m).

The number of MTDs corresponding to the event horizons varies from a single MTD (EHs A & G) to basin-wide amalgamations in which up to 8 individual MTDs merge (EHs C & F). The discrimination of individual MTDs in such complexes was based on the isopach maps, i.e., thicker accumulations at the slope base point towards local slope sediment sources (red arrows in Figure 3). The total MTD volumes range from 0.3 x 10^3 m^3 (EH-A) to 605 x 10^3 m^3 (EH-H; Figure 3; Table 1). The amalgamated MTD of the lowermost event horizon (EH-H) does not show the largest

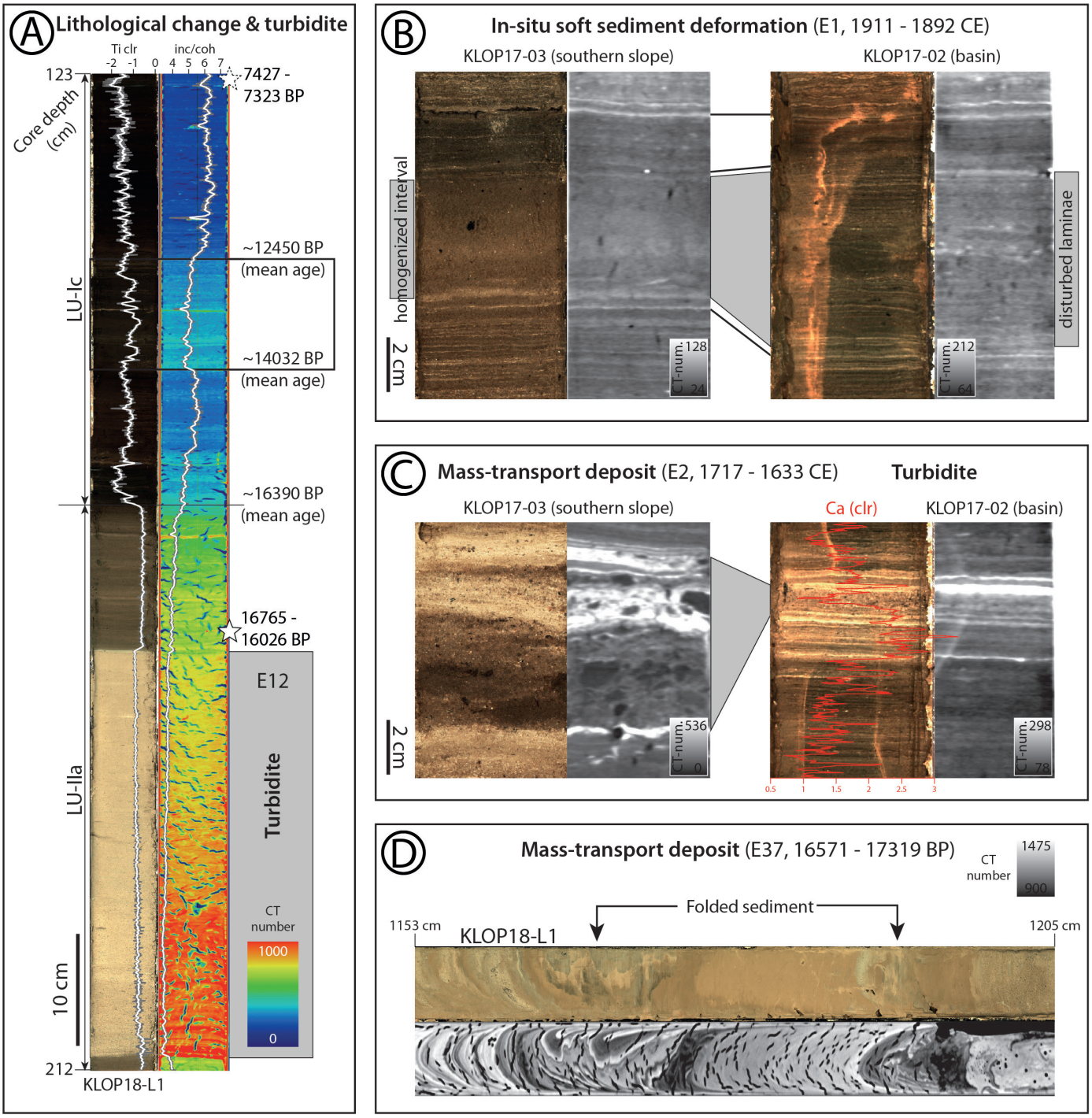

Figure 6 | Lithological changes and types of event deposits in Klopeiner See. (A) Transition from LU-Ic to LU-IIa. (B) Soft-sediment deformation structures are visible in the uppermost part of the short cores (see Figure 5A for location). Core correlation suggests that on slope cores, the otherwise laminated sediment was homogenized, while in the basin cores, the lamination was disturbed. (C) In LU-I, mass-transport deposits mostly consist of a mudclast-conglomerate. Distally, they can be correlated to turbidites. See Figure 5A for exact stratigraphical location within the short cores. (D) In LU-II, mass-transport deposits often show intervals of folded mud. See Figure 4B for exact stratigraphical location within long core KLOP18-L1.

thicknesses at the slope base, but in the central part of the basin where it deeply eroded into basin-plain sediments (irregular lower boundary of EH-H on Figure 2B). Small, single MTDs show source areas on the southern slope (e.g., EH-B, EH-D, EH-G) whereas large amalgamated MTDs were caused by basin-wide failure, i.e., involving slopes of different aspects.

4.2. Sediment core analysis

4.2.1. General lithostratigraphy

The general lithostratigraphy of core KLOP18-L1 consists of two lithological units, LU-I and LU-II, that differ strongly in macroscopic appearance, density, and lithological composition (Figure 4A, B, Supplementary Figure 4). LU-I is further subdivided into three sub-units, LU-Ia, LU-Ib and LU-Ic (Figures 4 and 5). LU-Ia consists of finely laminated (sub-mm scale) coarse silt with light yellowish

brown (2.5Y 6/3) to olive brown (2.5Y 4/3) colour. The brighter, yellowish laminae mainly consist of authigenic calcite and diatoms. The brownish laminae are mainly composed of amorphous organic matter and clayey to silty detrital particles. In accordance with the detailed sedimentological study and short-lived radiometric dating of similar laminations in Wörthersee (Daxer et al., 2022b), we interpret that the laminations are due to seasonal variations in authigenic calcite precipitation and therefore denote "calcite-rich" varves ("calcareous-organic varves" after Zolitschka et al., 2015). LU-Ib consists of very dark greyish brown (2.5Y 3/2), very coarse silt and in parts shows a fine, albeit faint, lamination as well. The main components are amorphous organic matter, diatoms, and accessory detrital particles. Authigenic calcite, however, is largely missing. The lamination arises from variations of the relative abundance of these components and the size of the minerogenic particles: spring and summer laminae are enriched in organic matter and silt-sized particles, while autumn and winter laminae mainly consist of clay-sized particles and are low in organic matter. The annual nature of these "organic-rich varves" is further attested by a ^{14}C-based age model on core KLOP17-01 (see section 4.2.4; Figure 5). Apart from a slightly higher abundance of large terrestrial plant macro remains (i.e., leave fragments) the composition of LU-Ic is similar to that of LU-Ib. However, the sediment is darker (2.5Y 2.5/1) and finely laminated intervals are less frequent than in LU-Ib or even absent. Within LU-Ic (139.5-149.5 cm core depth), an interval with high amounts of detrital components (quartz, feldspar, mica) and accessory amorphous organic matter, but with only sparse amounts of diatoms, is present. This compositional change is also reflected by higher densities and a lower incoherent/coherent scattering ratio (Figure 6A). At the transition to LU-II, the colour changes from black to grey and CT density rises abruptly (Figure 4B; 6A). Furthermore, titanium values rise and fluctuate less than in LU-I, while the values of Mo inc/coh decrease (Figure 6A). Based on colour and the presence/absence of macroscopically visible lamination, LU-II is further subdivided into four litho-units. LU-IIa consists of mostly homogeneous, dark greyish brown (2.5Y 4/2), coarse silt that is enriched in detrital particles, compared to LU-Ic. In LU-IIb, the detrital components of medium silt size (mainly detrital calcite/dolomite) are even more prominent and organic matter is largely missing (Supplementary Figure 4). The sediment is laminated on a mm-scale and is of grey colour (2.5Y 5/1). LU-IIc is compositionally identical to LU-IIb, but macroscopically almost homogeneous. CT scanning, however, reveals rhythmic graded laminae and beds on a mm- to cm-scale. Towards LU-IId, the greyish colour of the sediment transitions into light-yellowish brown (2.5Y 6/3) to light olive brown (2.5Y 5/3) tones, while the rhythmic beds and lithological composition persist.

4.2.2. Event deposits

Within the cored sedimentary succession, three different types of event deposits are present: turbidites, in-situ soft-sediment deformation structures (SSDSs) and MTDs (Figures 4B, 5 and 6). Turbidites are by far the most abundant type, with more than fifty turbidites over the whole cored composite section of KLOP18-L1. Turbidites can be included in the MTDs (e.g., in the MTD corresponding to EH-H; Figure 4B) and are then regarded as part of the same, single event deposit. Event deposits are named E1-E50 from top to bottom (Figures 4B and 5A). Depending on the lithostratigraphic unit in which they occur, their composition and colour varies, reflecting the respective background sedimentation (Figure 6A, C). Relatively thick turbidites (up to 30 cm) are frequent in

Event	LU	EH	Type	Age (mean)	Age (min)	Age (max)	Age (unit)	Amount of MTDs	Volume of MTDs (x 103 m^3)	Historical event?	Max. turbidite thickness (mm)	EQ trigger confidence
E1	LU-Ib	-	SSDSs	1901	1911	1892	CE	-	-	1899 CE EQ	-	Very high
E2	LU-Ib	EH-A	MTD/Turbidite	1679	1717	1633	CE	1	0.3	1690 CE EQ	10	Very high
E3	LU-Ib	-	Turbidite	2794	2480	3074	BP	-	-	-	4	High
E4	LU-Ib	-	Turbidite	3082	2924	3224	BP	-	-	-	14	High
E5	LU-Ib/c	-	Turbidite	3160	2996	3318	BP	-	-	-	1.6	Moderate
E6	LU-Ib/c	-	Turbidite	3160	2996	3318	BP	-	-	-	4.7	High
E7	LU-Ib/c	-	Amalgamated Turbidite	3160	2996	3318	BP	-	-	-	13	Very high
E8	LU-Ib/c	EH-B	MTD/Turbidite	3160	2996	3318	BP	3	12	-	16.5	Very high
E9	LU-Ic	-	Turbidite	3166	3002	3324	BP	-	-	-	1.7	Moderate
E10	LU-Ic	-	Turbidite	3323	3210	3422	BP	-	-	-	1.1	Moderate
E11	LU-Ic	-	Turbidite	4035	3696	4609	BP	-	-	-	5	High
E12	LU-IIa	EH-C	MTD/Turbidite	16542	16166	16913	BP	≥ 8	377	-	356	Very high
E16	?	EH-D	MTD/Turbidite	16894	16493	17247	BP	2	6	-	-	Very high
E18	LU-IIb	EH-E	MTD/Turbidite	16928	16528	17277	BP	4	97	-	385	Very high
E20	LU-IIb	EH-F	MTD/Turbidite	16944	16541	17292	BP	≥ 8	397	-	347	Very high
E22	LU-IIc	EH-G	MTD/Turbidite	16972	16571	17319	BP	1	22	-	134	High
E37	LU-IId	EH-H	MTD	17374	16961	17735	BP	≥ 6	605	-	-	Very high

Table 2 | Details of remarkable event deposits in Klopeiner See.

LUs IIa, IIb and IId, while in LU-IIc, turbidites are generally scarce.

In the composite core section of core KLOP18-L1, MTDs are characterised by strongly distorted and folded sediments (Figure 6D). Three such slumped sedimentary intervals are present in KLOP18-L1, occurring in LU-IId at about 10, 12 and 13.5 m composite depths (Figure 4B). The small number of MTDs recorded in KLOP18-L1 might be due to its very distal coring position. In the more proximal short core KLOP17-03, which only covers the uppermost 1.1 m of the sedimentary succession, two MTDs are present (Figure 5A). They consist of a heavily disintegrated, organic-rich mudclast conglomerate (Figure 6C).

In the uppermost part of some short cores, an interval of in-situ soft sediment deformation is visible (E1). In proximal cores (KLOP17-03 and KLOP17-08), the SSDS consists of strongly homogenized sediment (Figures 5A and 6B). In the basin cores (KLOP17-02 and KLOP17-01), intraclast breccias and disturbed lamination are present (Figure 6B).

4.2.3. Core-to-seismic and core-to-core correlation

Turbidites or lithological changes lead to abrupt shifts in the (CT) density of the sedimentary succession, which correspond to high-amplitude reflections in the seismic data. This allows for a detailed correlation between the lithostratigraphic succession and the seismic stratigraphy (Figure 4B). KLOP18-L1 covers seismic units 1 and 2 and barely reaches seismic unit 3. The calculated acoustic velocity from this core-to-seismic correlation is about 1400 m/s, which is lower than what is expected for fine-grained soft sediments (~1500 m/s). Such small discrepancy is often encountered in lake studies (e.g., Praet et al., 2022) and is caused by deformation and compaction processes during coring. The boundary between SU-1 and SU-2 corresponds to the increasing density at the LU-I/LU-II transition. The major seismostratigraphic event horizons either correlate to thick (~30 cm) turbidites (EHs C, E, F) or to the succession of MTDs and turbidites present in the sediment core from 10 to 13.5 m (EH-H). The minor seismostratigraphic event horizons A, B and G correlate to smaller turbidites or a succession of such (EH-B). For the two MTDs of EH-D, a corresponding event layer in the sedimentary succession cannot be determined with high confidence as no outstanding turbidites are present in the core interval. A potential correlation to a 0.5 cm thick turbidite at ~3 m core depth, however, is possible.

The presence of distinct marker layers together with a similar lithological succession allow short cores to be correlated along a south-north (Figure 5) transect. The correlation shows that the SSDSs in the proximal cores occur at the same stratigraphic interval as those in the distal cores. The MTDs consisting of organic-rich mudclast-conglomerates in the proximal cores further correspond to turbidites in the distal cores.

4.2.4. Chronology and event stratigraphy

The age-depth model of core KLOP18-L1 is based on seven radiocarbon ages of (terrestrial) organic remains retrieved from cores KLOP17-01 and KLOP18-L1 (Figure 4C, Table 1) and was extrapolated to the calculated sediment depth at the onset of glaciolacustrine sedimentation (16.3 m), which is presumed to have occurred at 18500 ± 500 cal BP (see section 2.3). The average sedimentation rates calculated from the age-depth model are rather low in litho-unit I (LU-Ia: ~0.8 mm/yr; LU-Ib: ~0.2 mm/yr; LU-Ic: 0.07 mm/yr) but rise drastically at the transition to LU-IIa (~1.4 mm/yr) and again from LU-IIa to LU-IIb (~10 mm/yr; Figure 4C). To circumvent potential uncertainties involved in the projection of ages to the composite section KLOP18-L1, a separate age-depth model based solely on the radiocarbon ages obtained from core KLOP17-01 was calculated for the interval covered by short cores (Figure 5). The uppermost ~30 cm of the sedimentary succession is also covered by a varve-based age-depth model (Figure 5A). Overlapping age ranges for the E2 event deposit between the ^{14}C-based model (1459-1689 CE) and the varve-based model (1633-1717 CE) further attest the annual nature of the laminations used for counting. These age-depth models allow for accurate dating of the event deposits and their respective seismostratigraphic event horizons (Table 2).

For long periods in the Klopeiner See record, event deposits are rare or absent. There are, however, two intervals of drastically enhanced event deposit frequency. The first of these event clusters occurred in Late Glacial times: our age-depth model suggests that four large events (EHs D-G) happened within the short period from ~16970-16890 cal BP (mean ages), i.e., within 100 years (Table 2). This event cluster is preceded and followed by the large events of EH-H at ~17370 and EH-C at ~16540 cal BP, respectively. Note that age control for the Late Glacial part of the record (LU-II) is affected by several factors: i) The timing of glacier retreat is derived from literature projected to the onset of glaciolacustrine sedimentation in the lake (section 2.3), ii) only two ^{14}C dates were obtained in LU-II, iii) the choice of an observational threshold of 5 cm for excluding event deposits from the event-free age-depth model of core KLOP18-L1. Such a high thickness threshold is justified for a proglacial lake due to the difficult distinction of a clastic turbidite from a clastic bed (up to 5 cm) that represents a year of high sedimentation rate (e.g., Praet et al., 2020).

The second event cluster comprises the events E5-E8, which are only separated by ~6 mm of background sediment in total (Figure 7). Thus, these events were not treated individually in the ^{14}C-age-depth-modelling process, but considered as one instantaneous event, leading to an age of ~3160 cal BP (mean age) for all four events. Given a lamination-thickness of ~0.1-0.2 mm (Figure 7C), E8 and E5 occurred within a period of 60 years maximum. This event cluster is followed by two prominent events (E4 and

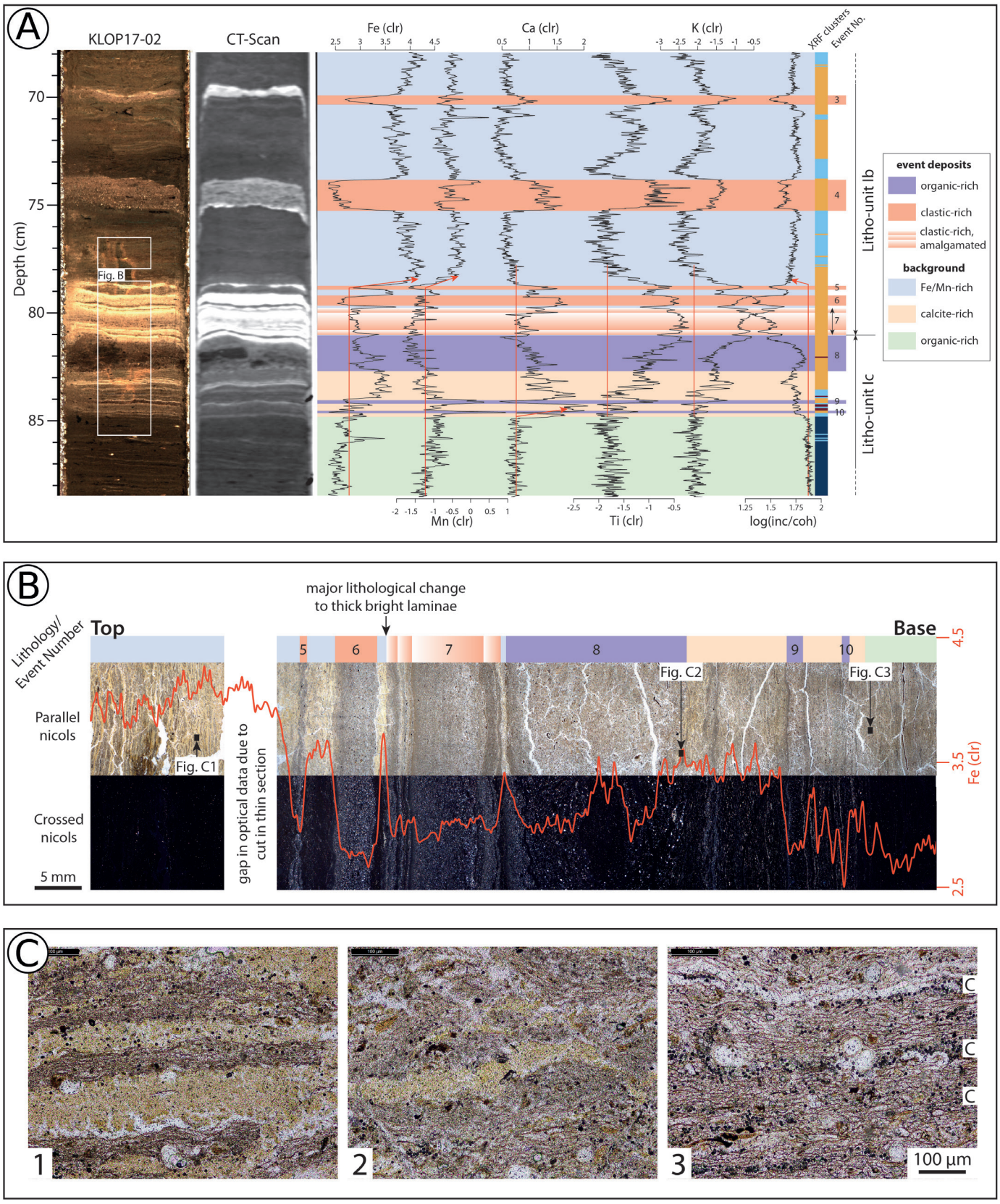

Figure 7 | Detailed description of the geochemical shift at ~3160 cal BP. (A) Core photograph, CT scan and XRF-data. (B) Detail of the event cluster at 80 cm sediment depth using sediment thin sections. (C) Thin section microscopic images of the sediment above (C1) and below (C2 & C3) event 8.

E3) at ~3080 and ~2790 cal BP. The uppermost events in the stratigraphic record happened in relatively recent times: event 2 (EH-A) is varve-dated to 1717-1633 CE, event 1 to 1911-1892 CE.

4.2.5. Geochemistry, cluster analysis and detailed description of the event cluster ~3160 cal BP

Multivariate analysis of the XRF data suggests the presence of four geochemically distinctive clusters in the short cores of Klopeiner See (Figure 5): cluster 1 (red) is characterized by high values in Ca, indicating authigenic

calcite precipitation (Croudace & Rothwell, 2015); cluster 2 (light blue) represents elevated values of the redox-sensitive elements Fe and Mn; cluster 3 (dark blue) is mainly representing sediments high in Si and light-weight elements (inc/coh scattering ratio); and cluster 4 (orange) is mainly characterized by indicators of detrital input such as Ti and K. The distribution of the clusters throughout the cores shows that the macroscopic observations used to derive the general lithostratigraphic succession are also reflected by the geochemical signal: LU-Ia consists almost exclusively of cluster 1, LU-Ib is mainly represented by cluster 2, LU-Ic almost entirely composed of cluster 3, and the turbidites and intervals of enhanced clastic input mainly correspond to cluster 4. The distinct geochemical change from cluster 3 to cluster 2 occurs just above the suite of events numbered E5-E8 and dated to ~3160 (2996-3318) cal BP.

Figure 7 provides a detailed view of the geochemical and lithological changes that occur around ~3160 cal BP. Before the suite of event deposits (i.e., stratigraphically below event 10), dark, organic-rich sediment is present. The indistinct lamination of this sediment arises from the rhythmic deposition of black laminae mainly composed of chrysophyte cysts (labelled "C") and brown laminae rich in amorphous organic matter. Just before event 10, the sediment starts to be enriched in Ca, but no distinct micromorphological change is visible in the thin sections. This Ca-rich interval spans about 2 cm of sediment just below E8 and is very similar in macro- and microscopic appearance to the calcite-laminae present below E2 (Figure 5). The onset of bright laminae (typical for the microscopic appearance of LU-Ib) occurs just below E8 (Figure 7C_2), with this type of lamination becoming dominant after the deposition of E8 and E7. The major geochemical change, i.e., the persistent change from XRF cluster 3 to cluster 2, occurs after the deposition of E5.

5. Discussion

5.1. Sedimentary evolution of the lake infill

The transparent to semi-transparent seismic facies of the acoustic basement together with an irregular, discontinuous reflection at the top is indicative of a subglacial deposit, i.e., till (Fabbri et al., 2018; van Rensbergen et al., 1998). Chaotic, but partly stratified parts of seismic unit 3 are interpreted as glacier-contact proglacial lake deposits that directly overly the glacial till. The well-stratified parts of seismic unit 3, found in the very depocenter of the lake and – in their uppermost part – corresponding to the olive-brown rhythmic beds of LU-IId, are interpreted as underflows in an ice-proximal environment. Other authors described similarly-coloured Late Glacial deposits in Lake Geneva (Baster et al., 2003), Lake Neuchâtel (Ndiaye et al., 2014) and Mondsee (Daxer et al., 2018). Nevertheless, Baster et al. (2003) attributed them to an aeolian origin. In Lake Geneva and Lake Neuchâtel, however, these deposits are of much younger age (Oldest Dryas) than in Klopeiner See. Because of the still largely ice-covered Alps during the time of deposition of these olive-brown layers in Klopeiner See (cf. Seguinot et al., 2018), an aeolian origin of these layers is therefore very unlikely. Throughout the deposition of LU-IIc, the ice margin remained relatively close to Klopeiner See, as indicated by the thick rhythmites. The east and northwards decreasing amplitudes in seismic unit 2 indicate the sedimentary deposition as underflows and an ice-margin position close to the west and south of Klopeiner See. Thinning glaciolacustrine laminae, as observed at the transition from LU-IIc to LU-IIb, are common observations associated with ice margin retreat (de Geer, 1912; Palmer et al., 2019; Ridge et al., 2012). It is therefore likely that at the transition from LU-IIc to LU-IIb (16900-16500 cal BP), the glacier started to retreat beyond the Rückersdorfer plateau and Klopeiner See was in a more distal position relative to the ice margin. The relatively quick glacial retreat and subsequent development of soils and vegetation is expressed in the increased amounts of organic matter found in LU-IIa, the timing of which is also consistent with the modelled ice-decay from ~17000-16000 cal BP (Seguinot et al., 2018). For example, the plant remains (needles of *Abies* sp., bark; Supplementary Figure 5) found at 192.4 cm core depth and dated to 16755-16025 cal BP indicate that the area surrounding Klopeiner See was forested very early. The main lithological change is denoted by the transition from LU-IIa to LU-Ic, dated to ~16390 (16830-15935) cal BP. The organic-rich gyttja-like sediments of LU-Ic indicate a complete detachment from any glacial influence. The slightly denser interval within LU-Ic dated to ~14030 to ~12450 cal BP might represent climatic variations during the Bølling-Allerød or the Younger Dryas. The age-depth-model presented in this study, however, is insufficient to resolve the exact timing of these minor lithological changes and this would also be beyond the scope of this study. The lake system remained in a state of dominantly organic-rich sedimentation until ~3160 cal BP, when the lithology and geochemistry abruptly changed. This interval (LU-Ib) is discussed in more detail in section 5.4. The deposition of the calcite-rich laminae in LU-Ia, which started about ~60 years ago, is a typical indication for human-induced eutrophication (e.g., Kienel et al., 2013). Due to extensive agriculture and other human activities, the phosphorus and nitrogen concentrations in lakes increased, leading to enhanced primary production by algae. The CO_2 removal during photosynthesis led to calcite supersaturation and subsequent deposition of calcite-rich laminae (Escoffier et al., 2023; Khan et al., 2021).

5.2. Trigger mechanisms of the observed event deposits

MTDs are the result of subaqueous mass movements, which can be triggered either spontaneously, especially on deltas (e.g., Girardclos et al., 2007; Hilbe & Anselmetti, 2014), or via rockfalls (Daxer et al., 2018; Kremer et al., 2012), lake-level fluctuations (Anselmetti et al., 2009), floods (Vandekerkhove et al., 2020) or earthquakes

(Schnellmann et al., 2002). At Klopeiner See, there is no indication of rockfall activity (e.g., subaqueous or onshore rockfall cones; cf. Schnellmann et al., 2006) or severe lake-level fluctuations during the Holocene (e.g., erosional surfaces in the reflection seismic data). Reported recent maximum lake level fluctuations are within 50 cm over several years (Messiner & Windisch, 2008). Given the small to non-existent surficial inflows and the relatively small catchment area, we estimate that sudden severe sediment loading during high-precipitation events (i.e., floods) and a subsequent (delta) slope failure is very unlikely. Spontaneous slope failures of deltas in Klopeiner See are as unlikely because extensive deltas with high sediment supply do not exist. Simultaneous failure of multiple slopes, as reported for several event horizons in Klopeiner See, is a strong indicator for a seismic trigger (also known as the "synchronicity criterion"; e.g., Praet et al., 2017; Schnellmann et al., 2002). We therefore attribute a very high earthquake-trigger confidence level to events recorded in Klopeiner See as multiple coeval MTDs (Figure 3; Table 2).

Lacustrine turbidites can either result from (1) mass movements and their transformation into a turbidity current, (2) the remobilization of the uppermost few centimetres of sediment during seismic shaking (Moernaut et al., 2017), (3) lake water seiching due to mass movements or seismic shaking, or (4) hyperpycnal flows associated with fluviatile sediment transport (i.e., floods due to heavy precipitation events or intense snowmelt; Heerema et al., 2020). As discussed above, very high river runoff is unlikely at Klopeiner See due to the very limited catchment size and its dense forest cover. As indicated by the terrestrial organic matter found at ~1.9 m core depth, this forest is present since at least 16000 cal BP. During the 9th century BCE (i.e., from ~2850 cal BP onwards), human activity is reported at the Gracarca (Gleirscher, 1996, 2009), just south of Klopeiner See. This might have led to the opening of the landscape to a minor degree, and therefore facilitated enhanced surface runoff. However, no increase in turbidite frequency is observed in the Klopeiner See sediments and the major event deposits of the Holocene occurred prior to the first reported human activity. During the strongest precipitation event since the installation of the hydrographical measurement station at Klopein (1899 CE; see Figure 1C for exact location) in July 1958, 90.2 mm of rain were measured during one day (Bundesministerium für Land- und Forstwirtschaft, Umwelt und Wasserwirtschaft, 2013). No traces of this event, however, are present in the sediment of Klopeiner See. Hence, even major precipitation events most likely only lead to very small event deposits in Klopeiner See that can only be observed on microscopic scale. Therefore, turbidites thicker than 3 mm are likely related to MTDs that are not resolved in the available 2D seismic or core data, to seiching, or to surficial sediment remobilisation. Thus, we attribute a high earthquake-trigger confidence level to turbidites recorded in LU-I that are thicker than 3 mm. While turbidites thinner than 3 mm might as well be triggered by earthquakes, a flood-origin cannot be completely ruled out. Therefore, we attribute only a moderate earthquake-trigger confidence level to these turbidites.

SSDSs in muddy sediments have been reported to be caused by seismic shaking (Molenaar et al., 2022; Sims, 1973), sudden gravitational overloading (Owen, 2003) or wave action (Molina et al., 1998). Because there are no signs of sudden deposition of large sediment volumes in the upper part of the cores (low sedimentation rates) and because wave loading on this small lake (small wind fetch) does not impact the deepest parts of the lake, we attribute a seismic trigger to the SSDSs found in the sediment cores of Klopeiner See.

5.3. Calibrating the lacustrine seismograph of Klopeiner See

Quantitative lake paleoseismology requires establishing a ground shaking threshold above which a specific type of imprint occurs in the sedimentary record. For this, it is common practice to compare the type and extent of earthquake-related imprints with the seismic intensities at the lake that were produced by historical and recent earthquakes (Moernaut, 2020). For the Klopeiner See area, there are no Intensity Data Points (IDPs) for the strong historical earthquake in 1511 CE and many IDPs for 1348 CE event have veracity/location problems and are debated (Caracciolo et al., 2015, 2021; Hammerl, 1994). Therefore, we only use the calculated local seismic intensities based on magnitude and epicentral distance to calibrate the sedimentary archive. The advantage is that the epicentre location and magnitude was determined based on a high number of IDPs (90 for 1348 CE; 122 for 1511 CE) and thus somewhat levels out the potential influence of some ambiguous or poorly-quantified IDP values. We calculated local intensity based on both the SHEEC and EPICA catalogues and report both values here.

The mean varve age of the SSDSs (E1) found in the short cores of Klopeiner See is 1901 CE, with an error range of 1911-1892 CE. Two earthquakes with local intensities > V are reported for the vicinity of Klopeiner See during that time: the 1895 CE Ljubljana earthquake (M_w ~5.9 ± 0.3), which led to calculated local intensities of V-VI¼ (SHEEC and EPICA) at Klopeiner See, and the 1899 CE earthquake (M_w ~4.9 ± 0.5) that occurred within ~13 km of Klopeiner See with calculated local seismic intensity V½-VII (SHEEC and EPICA) and reported seismic intensity at the lake of VI-VII. Because of the higher local seismic intensities of the 1899 CE earthquake compared to the 1895 CE earthquake, and the observation made in other lakes that SSDSs occur at intensities >VI (Monecke et al., 2004; Oswald et al., 2021), the 1899 CE earthquake is more likely to be the causative earthquake for the reported SSDSs in Klopeiner See.

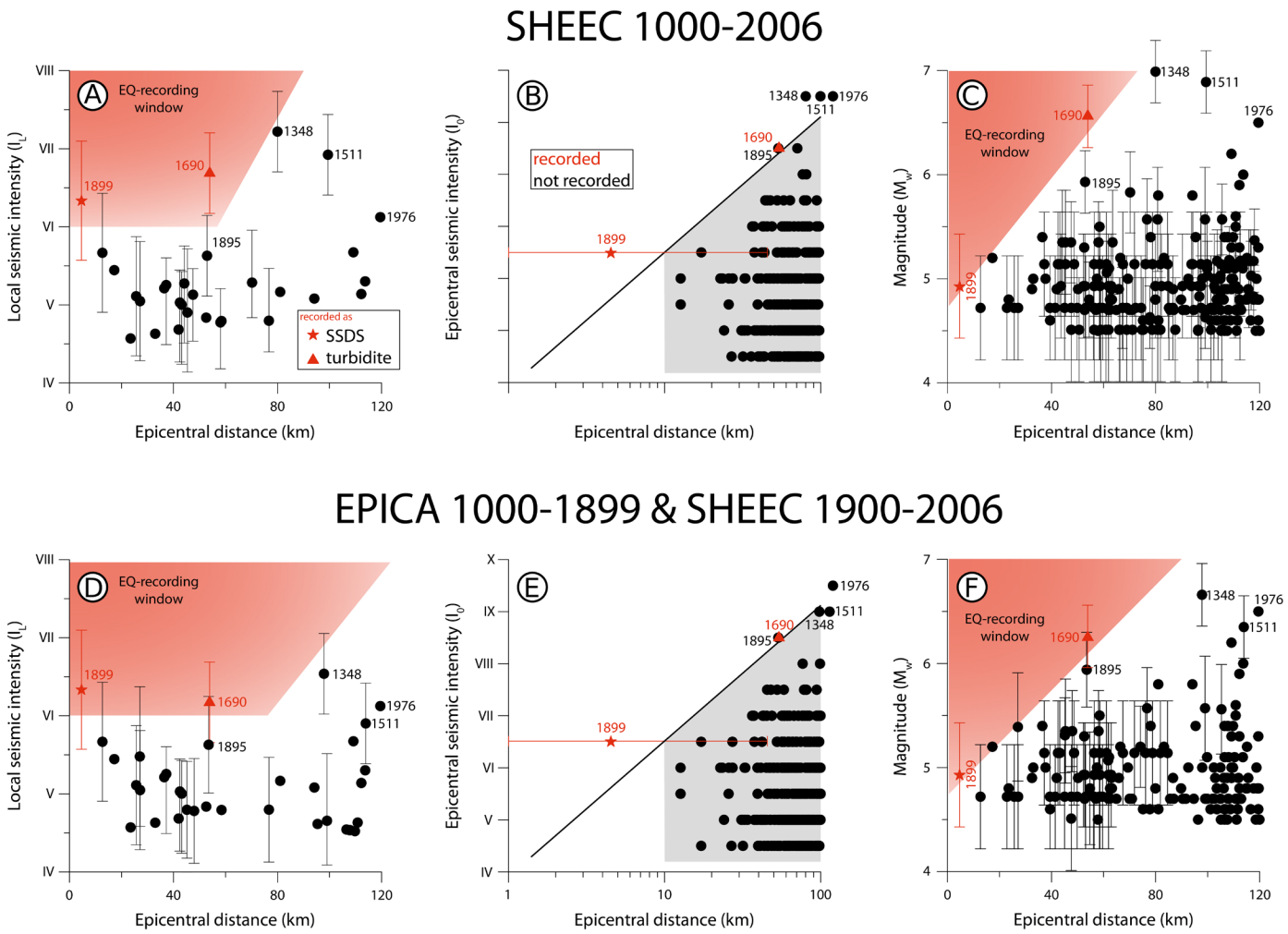

Figure 8 | Calibration of the Klopeiner See paleoseismic record. In (A) to (C) the pre-instrumental data (i.e., pre 1900 CE) is based on SHEEC (Stucchi et al., 2013), in (D) to (F), the pre-instrumental data is based on EPICA (Rovida et al., 2022). The vertical error bars indicate the uncertainty concerning the magnitude of the earthquakes (C) & (F) as given in the earthquake catalogues, which also impacts on the uncertainty of the calculated local seismic intensities (A) & (D). (A) & D) Epicentral distance vs. local seismic intensity (I_L). (B) & (E) Epicentral distance vs. epicentral seismic intensity ("earthquake sensitivity index", i.e., ESTI) plot after Wilhelm et al., 2016). For comparability, the slope of the threshold line is the same as in the previous studies that used the ESTI (1.31; Daxer et al., 2022b; Rapuc et al., 2018; Wilhelm et al., 2016). (C) & (F) Epicentral distance vs. moment-magnitude.

The only other event that falls into the historical period is E2, consisting of an MTD and turbidites and varve dated to 1717-1633 CE with a mean age of 1679 CE. As previously discussed, triggering factors other than earthquakes are very unlikely for MTDs in Klopeiner See. Thus, the 1690 CE earthquake (M_w ~6.3-6.6 ± 0.3), which produced a local seismic intensity of VI¼-VII¼ (SHEEC) / V¾-VI¾ (EPICA) at the lake, is the most likely triggering event. We therefore conclude that both the 1899 CE and the 1690 CE earthquakes are recorded in Klopeiner See, whereas earthquakes with local seismic intensities lower than ~VI are generally not. Thus, the earthquake-recording threshold (EQRT) of Klopeiner See, i.e., the seismic intensity above which seismically triggered MTDs, turbidites and SSDSs can be expected, is estimated to be around VI (Figure 8A).

The major earthquakes of 1348 CE (M_w 6.7-7 ± 0.3), 1511 CE (M_w 6.3-6.9 ± 0.3) and 1976 CE (M_w 6.5) are not recorded in the sediments, although local seismic intensities are calculated to be VI¾-VII¾ / VI-VII, VI½-VII½ / V½-VI½ and VI, respectively. Using the more recent EPICA catalogue, the I_L for 1511 CE (V½-VI½) could fall under the intensity threshold of VI, potentially explaining why there is no sedimentary imprint. The 1976 CE event has a calculated local intensity value of VI and also potentially just falls below the threshold. This is further supported by the lower IDPs of V nearby Klopeiner See in 1976 CE, indicating that our calculated intensity for this event may be an overestimation. For the 1348 CE earthquake, however, the calculated I_L (VI¾-VII¾ / VI-VII) is well above the threshold and represents the highest I_L of all historical earthquakes that struck Klopeiner See. Several arguments are explored to explain the absence of an imprint in 1348 CE:

i) Uncertainty in the earthquake source parameters: the reliability of many IDPs for the 1348 CE event has been strongly debated based on re-evaluation of the historical documentation (summarized in Caracciolo et al., 2021). As a consequence, all IDP values (VIII-IX) near our study area from the SHEEC catalogue are changed in the EPICA catalogue to "High Damage" with "veracity problems".

This affects the calculated M_w and epicentre location and therefore also the I_L at Klopeiner See, which indicates that I_L values for ancient events need to be regarded with caution. Nevertheless, the very large sedimentary imprint in Wörthersee in 1348 CE(i.e., the largest imprint for the entire Holocene; Daxer et al., 2022b), the high and reliable IDP value of IX-X in Villach (SHEEC and EPICA), and the large-scale rockslides at the Dobratsch mountain (Lenhardt, 2007) all suggest severe shaking near Villach.

ii) Directivity effects: the spatial pattern of strong ground motion can be affected by fault rupture dynamics, and is especially relevant in the case of unilateral fault rupture (Tiberi et al., 2014) and $M_w \geq 6.75$ (Sbarra et al., 2023). Seismic waves traveling in the direction of fault rupture typically have higher amplitudes and higher frequencies compared to seismic waves perpendicular to the fault rupture, leading to higher seismic intensity. As not even the causative fault for the 1348 CE earthquake is conclusively identified, such potential directivity effects were not yet implemented in the estimation of earthquake source parameters and in our I_L calculations.

iii) Change in the lake record sensitivity: A compilation of Alpine lake paleoseismic records shows that the sensitivity of a lake to record seismic shaking in its sedimentary archive can be strongly controlled by sedimentation rate (Wilhelm et al., 2016) and temporal changes in sedimentation rate may thus affect the frequency of seismo-turbidites in a record (Gastineau et al., 2021; Rapuc et al., 2022). The age-depth model of Klopeiner See shows higher sedimentation rate in the last ca. 400 years (0.5 mm/yr) compared to the preceding 2000 years (0.2 mm/yr). An associated increase in sensitivity (decrease in intensity threshold) could potentially explain why the 1348 CE event was not recorded, whereas a clear imprint for the 1690 CE event is present. However, this explanation is speculative at best as the change in sedimentation rate is constrained by only one ^{14}C date and does not include the fact that organic-rich shallow sediments are much less compacted than the underlying ones. Moreover, the amount of accumulated slope sediments after the last major events (at ~2500-3300 cal BP) would only be a few cm more in 1690 than in 1348, and thus would not significantly affect slope stability.

iv) Epicentral distance affects the ground motion characteristics: Our comparison between sedimentary imprints and historical earthquakes (Figure 8) suggests that seismic intensity on its own cannot explain the distribution of positive and negative evidence. In fact, for events with I_L >~VI, only the 1899 CE and 1690 CE events with an epicentral distance of ~5 and ~54 km are recorded, whereas the more remote (>75 km) and potentially higher M_w events in 1348, 1511 and 1976 CE are not recorded (Figure 8A, D). This suggests that the Klopeiner See record has a specific "earthquake-recording window" that depends on local intensity (horizontal threshold on Figure 8A, D) as well as on distance (inclined threshold line on Figure 8A, D). The latter contrasts with a distance-independent intensity threshold that is commonly suggested for a specific imprint in other lake settings and systems (Howarth et al., 2016; Kremer et al., 2017; Moernaut et al., 2014). Such control by epicentral distance is also supported by the magnitude versus epicentral distance plot, in which a sloping straight line separates all positive and negative evidence (Figure 8C, F). A possible explanation for these observations is that macroseismic intensity does not directly account for the frequency content of shaking, which is significantly affected by the travel distance of the seismic waves. Because the high-frequency component of earthquake ground motion attenuates faster (Jackson & Anderson, 1970), distant earthquakes cause shaking of relatively lower frequencies. This is in line with lacustrine paleoseismic studies in different settings which suggest that the triggering of lacustrine SSDSs, MTDs and turbidites is sensitive to the relative frequency content of the seismic shaking (Molenaar et al., 2021; Praet et al., 2022; Van Daele et al., 2019).

The four arguments presented here provide insights into the uncertainties of calibrating a lake paleoseismic record with historical earthquakes, especially regarding the historical earthquake data, changes in the recording sensitivity of the lake, and the nature of seismic wave propagation. It is currently not feasible to quantify these uncertainties and rank them in order of importance. With only one basin and low Holocene sedimentation rates, we can conclude that Klopeiner See probably is less suited than the lakes Wörthersee and Millstätter See for quantitative paleoseismology in Carinthia (Daxer et al., 2022b). Klopeiner See seems however, to be a valuable paleoseismological archive for local events, such as in 1690 CE and 1899 CE, but cannot readily be used for determining negative evidence for high intensity shaking that originate from more remote earthquakes (>75 km), and thus should be used with caution for regional paleoseismology studies (e.g., Kremer et al., 2017).

5.4. Implications for regional paleoseismicity

Three of the main historical earthquakes in the broader study area, i.e., in 1348, 1511, 1690 CE, are not only recorded in the Carinthian lakes Millstätter See and Wörthersee (Daxer et al., 2022b), but also in Lake Bohinj located in the Julian Alps, 65 km SW of Klopeiner See (Rapuc et al., 2018). This is expected due to the relatively short distance between Lake Bohinj and the estimated epicentres (Fig.1), i.e., ~50 km for the 1348 CE event, ~50 km for the 1511 CE event and ~38 km for the 1690 CE event. Lake sedimentary evidence is thus identified over an area of at least 1600 km^2 for 1348 CE and 1511 CE, and 2100 km^2 for 1690 CE. According to the Environmental Seismic Intensity Scale (ESI-07; Michetti et al., 2007), an epicentral intensity of about IX can be estimated for such an area affected by secondary earthquake effects, which is similar to the reported epicentral IDPs (EPICA). Remarkably, the M_w 6.5 event in 1976 CE did not leave an imprint in Lake Bohinj even though the epicentral distance is only 55 km

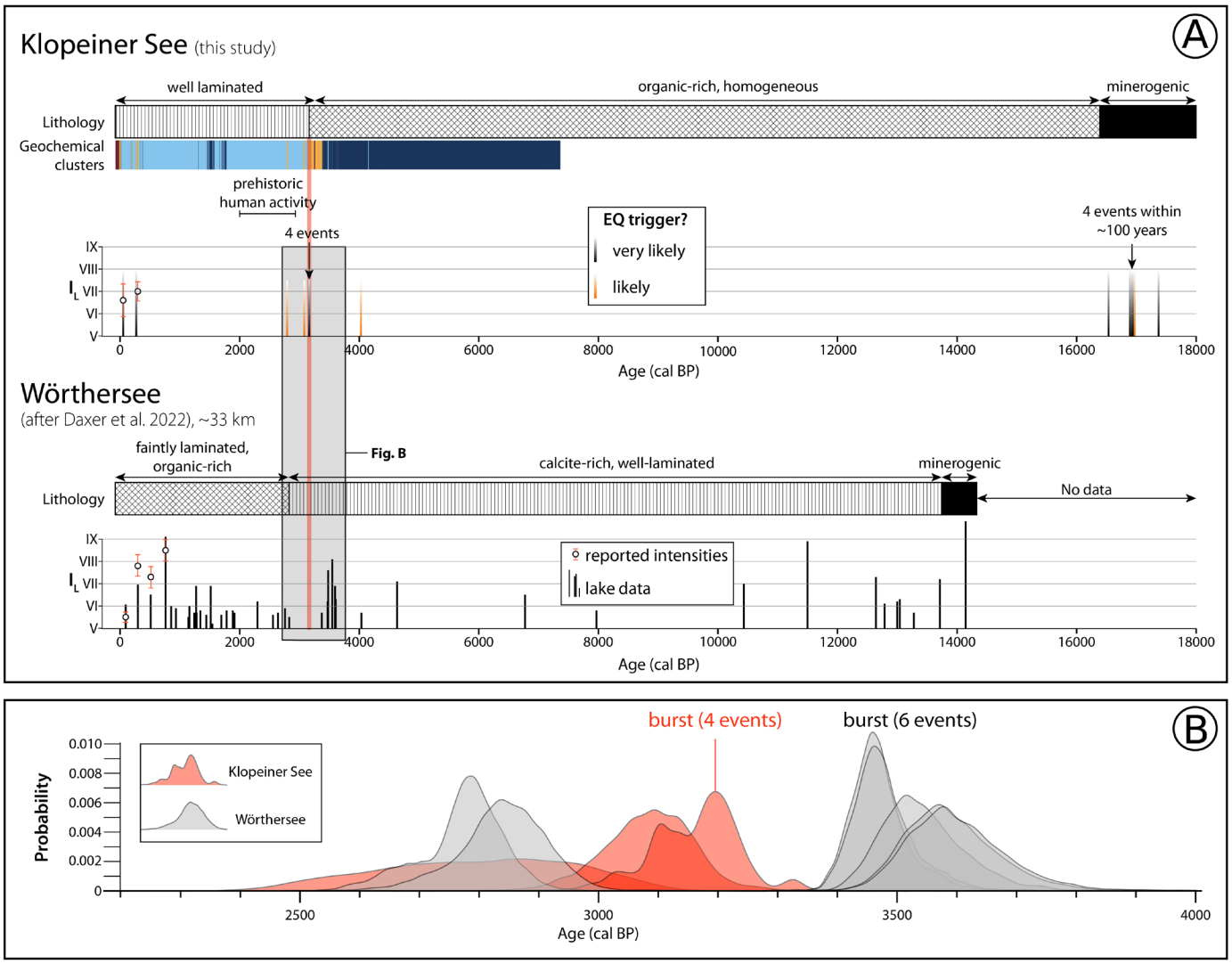

Figure 9 | (A) Comparison of the Klopeiner See paleoseismic record and lithology to the regional lake record of Wörthersee (Daxer et al., 2022a). For the uncertainties regarding the local seismic intensities (I_L) of historical earthquakes at Klopeiner See, see Supplementary File 1. (B) Histograms of modelled age distributions of earthquakes recorded in Klopeiner See (red) and Wörthersee (grey) at ~2500 to 4000 cal BP.

and IDPs reach ~VI-VII near the lake. Anthropisation of the lake banks is put forward as explanation of this negative evidence, but detailed studies are lacking (Rapuc et al., 2018).

The Klopeiner See data shows two episodes of high paleoseismic activity at ca. 16500-17500 cal BP in the Late Glacial and at ~3160 cal BP in the Late Holocene. Periods of enhanced mass-wasting in lakes are often found during the Late Glacial and are considered to be linked to increased seismic activity due to stress changes caused by ice sheet removal and/or subsequent isostatic uplift (Banjan et al., 2023; Brooks, 2018; Jakobsson et al., 2014; van Loon et al., 2016). For the Late Holocene (Figure 9), a link to isostatic rebound is much less plausible. We interpret the four paleoseismic events recorded in Klopeiner See that occurred within a short period of ~60 years (dated to 3318-2996 cal BP) to represent a short period of enhanced local seismicity (subsequently referred to as the "~3160 cal BP seismic burst"). It follows a seismic burst with six events at 3607-3471 cal BP recorded in the sediments of Wörthersee (Figure 9; Daxer et al., 2022a). This apparent age discrepancy is surprising as the studied basins lakes are only 33 km apart, and large earthquakes may impact the sedimentary record of both basins simultaneously. For example, the 1690 CE (M_w ~6.2-6.5) earthquake produced a MTD volume of 21 x 10^3 m^3 at Wörthersee and one of the few Holocene imprints at Klopeiner See. Age control in both records is considered to be adequate around 3000-4000 cal BP given the high density of ^{14}C samples and the well-identified macrofossil sample material for ^{14}C dating. However, it cannot be fully excluded that ^{14}C-dated material has been reworked, which could lead to age overestimations. If this applies to some of the Wörthersee ages, this opens the possibility that the identified event deposits during both "bursts" relate to the same earthquakes. In case our ages are accurate however, a significant attenuation of seismic intensity with distance is required to explain the negative evidence at Wörthersee during the burst recorded at Klopeiner See, and vice versa. This is feasible as, for example, a shallow (<7 km) M_w 5.5 earthquake at Klopeiner See would generate an epicentral I_L of VII-VIII –much higher than the threshold value of Klopeiner See– and I_L of V½-VI½ at Wörthersee

(calculations after Fäh et al., 2011, see Supplementary File 1). The latter is close to the threshold value of most long core sites in Wörthersee and shaking could have been too weak to generate an imprint there. Another exemplary scenario that is consistent with the data would be a M_w 6 event 20 km east of Klopeiner See, which likewise also leads to I_L VII-VIII at Klopeiner See and I_L V½-VI½ at Wörthersee. Analysis of macroseismic data in Austria shows that most events in Carinthia occur at about 4 km depth (Lenhardt et al., 2007) and thus the application of the "shallow" earthquake formulas (<7 km depth) of Fäh et al. (2011) is justified for the abovementioned I_L calculations. Comparison of the 3160 cal BP seismic burst to the Lake Bohinj record (65 km SW of Klopeiner See) is complicated because it shows a drastic change in sedimentation type and rate at ~3500 cal BP, probably changing the frequency and composition of turbidites between 3500 and 2000 cal BP.

The Obir cave is only 11 km south of Klopeiner See and recorded two paleo-earthquakes during the Holocene, i.e., a fault slip event between 10730 ± 230 and 8610 ± 150 cal BP, and a speleothem damage event between 6280 ± 240 and 5700 ± 1200 cal BP (Baroň et al., 2022). The fault slip event has an estimated M_w 5.5 and the speleothem damage event may even have been stronger (M_w 5.5-7). None of these two events is recorded in the sediments of Klopeiner See even though a M_w 5.5 event at Obir cave would lead to I_L VII at the lake, well above the intensity threshold of VI obtained from historical earthquake calibration. This implies that Klopeiner See was incapable of recording strong shaking in its sedimentary archive during the Early and Middle Holocene. However, at ~3160 cal BP it did record several events in short succession. As sedimentation rates (and thus lake paleoseismic sensitivity) did not increase much before that time (from 0.15 mm/yr to ~0.25 mm/yr), this could be explained by particularly strong shaking (>VII) at Klopeiner See during the burst at 3160 cal BP, which is consistent with the example scenarios of a M_w 5.5 local earthquake at Klopeiner See or a more eastern M_w 6-type earthquake. However, without any information on the "presumed" faults that are mapped in the broader area of Klopeiner See, it is difficult to assign such scenarios to specific source fault sections. To do so in future work, field mapping of local faults, improved age control on the paleoseismic events, and additional paleoseismic records are required to better characterize the identified seismic bursts, and to enable calculations of potential epicentre locations and magnitudes to infer the most likely fault section ruptures (Kremer et al., 2017; Vanneste et al., 2018).

5.5. The ~3160 cal BP event cluster and long-lasting geochemical changes

As described in section 4.2.5, we observe several changes in the vicinity of the ~3160 cal BP event cluster. These include (1) geochemical changes: an increase in Fe and Mn and decrease of inc/coh and Si after the event deposits, as well as elevated Ca-values just below the thickest event deposit E8; (2) changes in lamination: from faint, only microscopically visible lamination based on the abundance of chrysophyte cysts before the event cluster to well-laminated sediment consisting of bright, Fe/Mn-rich laminae and organic-clastic-rich sediment after the event cluster; and (3) ecological changes: after the event cluster, an overall decrease in the abundance of chrysophyte cysts and leaf fragments can be observed. The observation that indicators for clastic sediment input, such as Ti or K, did not change at the transition from LU-Ic to LU-Ib suggests that the abovementioned changes relate to lake-internal processes.

The presence of calcite in lake sediments is not only controlled by clastic input and (biogenically mediated) authigenic calcite precipitation, but also by potential subsequent calcite dissolution, which might occur both in the water column and after deposition (Müller et al., 2006; Ohlendorf & Sturm, 2001). Calcite dissolution is closely linked to the decay of organic matter due to benthic microbial respiration (Müller et al., 2003; Wachniew & Rózański, 1997), which causes a lowering of the pH in the bottom water (as observed in Klopeiner See; Messiner and Windisch, 2008) and within the uppermost few centimetres of the sediment (Archer et al., 2019; Archer et al., 1989; Oxburgh & Broecker, 1993; Sulpis et al., 2017). The disturbance caused by the sudden sedimentation of a few cm-thick detrital layer (i.e., a mass-flow or turbidite) may cause changes in the benthic faunal assemblages (Bigham et al., 2021) and a decrease in microbial respiration (Harrison et al., 2018). This might lead to an increase in pH (Cai et al., 2010), prohibiting the dissolution of calcite in the sediments just below the event deposits E2 (Figure 6) and E8 (Figure 7).

The abundance and stability of iron- and manganese-rich precipitates in lake sediments is often linked to seasonal changes in the redox conditions of the lower water column and the sediment surface, with an underlying process of spring and autumn circulation, which oxidizes Fe^{2+} to Fe^{3+} and then deposits it as $Fe(OH)_3$ (Ojala et al., 2013). This leads to light-coloured $Fe(OH)_3$-layers that form at the time of deposition (Gälman et al., 2009) and can be permanently preserved, even with changing redox conditions in the following years (Shchukarev et al., 2008). At Klopeiner See, seasonal precipitation of Fe-oxides and Mn-oxides is required to explain the different varve composition and thus more pronounced laminations in Litho-unit Ib compared to Litho-unit Ic (Figure 7C). This is supported by the corresponding increase in Fe and Mn content on the XRF scanning data. Permanent oxygenation of the bottom water can be excluded as this would allow macrobenthic organisms to bioturbate the sediments and fine laminations would not have been preserved.

Chrysophytes, commonly known as golden or golden-brown algae, are an important part of algal communities in freshwater systems (Wehr & Sheath, 2003). Under

unfavourable environmental conditions, they form siliceous resting stages (cysts), which can be preserved in lake sediment. Several studies show that chrysophyte cyst assemblages and their overall abundance are highly influenced by mixing patterns, summer stratification of the water column, and redox conditions (Hernández-Almeida et al., 2015; Szczerba et al., 2023). We interpret the decrease of Si observed within the XRF data after the event cluster to be caused by the overall decrease of chrysophyte cyst abundance.

Altogether, these observations indicate that at the transition from Litho-unit Ic to Litho-unit Ib, the seasonal variability within the lake system increased and remained as such permanently. Currently, Klopeiner See is mainly fed by groundwater that enters the southern part of the lake at 30-46 m water depth where it dilutes the hypolimnion with oxygen and allows FeS at the lake bottom to be oxidised to $Fe(OH)_3$ or Fe_2O_3 (Messiner & Windisch, 2008). We hypothesize that a significant increase in this lake spring activity (see section 5.6), producing seasonal oxygenation of the bottom water, is the main cause of the abovementioned lake-internal changes that occurred at ~3160 cal BP. This mechanism would not only form a straightforward explanation for the increased Fe and Mn contents, but also for the decrease in organic matter content (lower inc/coh ratio and less leaf fragments) as there would be more aerobic degradation and less preservation potential of organic matter.

5.6. Implications for paleoseismology in small groundwater-fed lakes

Once cut-off from direct sediment input via glacier meltwater streams, small lakes with a small catchment often show a dramatic change in sedimentation rates and style at the transition from the Late Glacial to the Holocene, i.e., from rapidly deposited glaciolacustrine silts to very slowly accumulating gyttja sediments (Brooks, 2018; Ojala et al., 2019). This transition in sediment dynamics has large effects on the earthquake-recording potential and the type of potential earthquake imprints. While an MTD-stratigraphy may form a complete record for Late Glacial times in small lakes, seismic imprints in the organic-rich Holocene sediments are often absent or very subtle and can remain undetected. For example, the period 16300-4200 cal BP does not show any detectable earthquake imprints in Klopeiner See, whereas a very high intensity event (I_L ~X) was recorded at 14100 cal BP in the nearby lake Wörthersee (Daxer et al., 2022a) and seismic shaking at Klopeiner See must have been severe. This implies that periods that show an absence of earthquake imprints in slowly deposited organic-rich lake sediments cannot be used as negative evidence for strong seismic shaking (see also section 5.3). Hence, caution is needed when modelling potential epicentre locations and magnitudes based on regional lake paleoseismic compilations that contain such non-ideal lake systems (Kremer et al., 2017; Oswald et al., 2022). This also implies that the timing of cut-off from glacier meltwater streams forms a crucial point in the depositional history of a lake and its potential use for paleoseismology. Sedimentation rates in proglacial lakes are typically very high and thus paleoseismic records can be very sensitive (Praet, 2020; Praet et al., 2022). However, conventional coring techniques fail to recover more than a few thousands of years in those units due to the limited attainable coring depth. Consequently, depending on when the transition in sediment dynamics occurred, one retrieves a high-quality Late Glacial paleoseismic record for only a specific period.

In Wörthersee and Klopeiner See, the transition point occurred at ~13800 cal BP and ~16400 cal BP, respectively (Figure 9). For Klopeiner See, which is located near the eastern edge of the LGM ice extent, we thus obtain a window into Late Glacial paleoseismicity between 17300 and 16400 cal BP (i.e., the base of core KLOP18-L1), which reaches back in time as far as the Lake Zurich record (Strasser et al., 2013) and significantly more than most other lake paleoseismic records in the European Alps (e.g., Kremer et al., 2020; Rapuc et al., 2018). The drawback is that a direct comparison of Late Glacial paleoseismicity recorded in Wörthersee and Klopeiner See is hampered.

As the subtle earthquake imprints for organic-rich Holocene sediments can come in a wide variety, it is necessary to not only investigate gravity-driven deposits, but also SSDSs (Oswald et al., 2021), seismic seiche deposits (Avşar et al., 2014) or even ecological indicators (Brancelj et al., 2012). Based on our present study, we propose to add permanent geochemical changes in groundwater-fed lakes to this list of lake paleoseismic indicators. At Klopeiner See, the synchronicity of the earthquake-triggered event deposits E5-E8 and the long-lasting sudden change in geochemistry suggest a causative link. We combine all data and first-order interpretations (section 5.5) to propose a conceptual model in which strong earthquake shaking at ca.~3160 cal BP induced a sudden connectivity increase in the hydrogeological system that feeds Klopeiner See. Since then, an increased seasonal input of oxygenated bottom water allows Fe- and Mn-oxides to precipitate and be preserved in the sedimentary sequence.

Such earthquake-triggered hydrogeological changes are commonly reported for recent and historical earthquakes (Barfal et al., 2022; Wang & Manga, 2015 and references therein), but to our knowledge, this is only the second study (next to Archer et al., 2019) that proposes that this signal can be preserved and traced in a lake sedimentary record and potentially can be used for paleoseismic purposes. As outlined on the Environmental Seismic Intensity Scale (ESI-07; Michetti et al., 2007), seismically-induced changes in spring activity become common at Seismic Intensity VII-VIII and above, which is above our threshold of VI (for distance <60 km) at Klopeiner See for generating event deposits that are associated with the seismic burst around ~3160 cal BP (section 5.3), and which would be reached by the scenario of a local M_w 5.5 earthquake at the lake.

In Hall in Tirol, located in the Eastern Alps, a M_w 5.5 ± 0.3 earthquake in 1670 CE (EPICA database) led to an epicentral intensity of VII-VIII and affected several springs in the vicinity: some ran dry whereas the flow rate changed in others (Hammerl, 2017), indicating that a M_w 5.5 earthquake in the setting of the Eastern Alps potentially can affect local groundwater systems.

In general, local earthquakes have a higher potential to directly and persistently affect the local hydrogeological system compared to high magnitude remote earthquakes, because local events may produce coseismic ruptures that lead to changes in groundwater flow paths or the formation of new springs (Wang & Manga, 2015). Furthermore, in the near and intermediate field, earthquakes cause changes in both static and dynamic crustal stress within the hydrogeological catchment, whereas in the far field, only dynamic stress changes occur (Manga & Wang, 2015). In addition, the associated ground motion of nearby earthquakes may contain a higher proportion of high-frequency components which are more detrimental to rocks (Song et al., 2019). An interesting example in the European Alps is found on the bottom of Lake Neuchatel in Switzerland (Reusch et al., 2016; Reusch et al., 2015) where sediment overflows from spring pits attest for enhanced subaqueous spring activity following paleo-earthquakes that are proposed to have originated in the nearby Jura Mountains. In contrast, strong shaking (local intensity VI-VII) by the more remote high-magnitude (M_w 6.6) Basel earthquake in 1356 CE did not leave any sedimentary imprint near the subaqueous springs. The above arguments let us hypothesize that the inferred hydrogeological change at ~3160 cal BP in Klopeiner See was caused by at least one local earthquake (M_w 5.5 type) in the direct vicinity of the lake, however evaluating a potential source fault is not feasible yet (see discussion section 5.4).

Altogether, our interpretations of the Klopeiner See Holocene record point towards a dominant control of local over remote earthquakes for producing earthquake-triggered event deposits as well as hydrogeologically-related geochemical changes in a small lake that is mainly fed by groundwater. Limnogeological research on other similar lake systems in active tectonic settings is required to evaluate the broader applicability of our results. Specifically, it is necessary to determine whether intensity thresholds for lake paleoseismology can be distance-dependent and whether ground-water fed small lakes can provide a unique view on the occurrence and effects of local, low magnitude earthquakes (M_w 5.5 type), which are difficult to study with other paleoseismic techniques such as on-fault trenching.

6. Conclusions

In this study, we document subaqueous landslides, soft sediment deformation structures and geochemical changes related to seismic shaking in the groundwater-fed lake Klopeiner See, located in the slowly deforming region of the Eastern European Alps. We draw the following conclusions:

- The potential for triggering subaqueous landslides and turbidity currents by strong seismic shaking is strongly dependent on the rate and type of sedimentation on the lacustrine slopes. Therefore, the sedimentary record of glacier-fed lakes can contain extensive mass-transport deposits and numerous turbidites, whereas earthquake imprints in small basins with small catchments are rather subtle. Due to deglaciation of their catchments, many lakes show a sudden transition in type and abundance of paleoseismic evidence.

- The Klopeiner See record forms an apparently inconsistent archive of strong historical earthquakes. This could relate to uncertainties in the earthquake source parameters, the nature of seismic wave propagation or temporally changing sensitivity of the lake system to record seismic shaking. However, our data suggest that the presence of earthquake imprints is a function of local intensity as well as distance to the seismic source. This contrasts with a constant intensity threshold typically proposed for MTD and turbidite records in large, deep lake basins with significant catchment areas. Potentially, the sediments in Klopeiner see can form a complementary paleoseismological archive for local events, but may fail to record high intensity shaking originating from high-magnitude far-field earthquakes.

- A seismic burst consisting of four earthquakes around 3160 cal BP is present in the sedimentary archive of Klopeiner See. This sequence of events occurred within ca. 60 years. The event cluster coincides with a drastic shift in the geochemical signal within the sediment. We attribute this to a permanent change in groundwater pathways during seismic shaking, potentially triggered by a local earthquake. Such geochemical shifts in groundwater-fed lakes may form a new indicator for paleoseismic activity.

Acknowledgements

This research was funded in whole or in part by the Austrian Science Fund (FWF) [10.55776/P30285]. For open access purposes, the author has applied a CC BY public copyright license to any author accepted manuscript version arising from this submission. Moreover, it received funding via the Austrian Academy of Sciences project "S4SLIDE-Austria". CD acknowledges financial support from a research grant from the University of Innsbruck (Exzellenzstipendium für Doktoratskollegs). KW acknowledges the financial support of the Research Foundation – Flanders (FWO, fellowship 12ZC422N). IHS Markit is acknowledged for their educational grant program providing the Kingdom seismic interpretation software. We thank ETH Zurich (Adrian Gilli) for access to the "Helvetia" coring system

and platform, Irka Hajdas for radiocarbon analysis as well as Markus Erhardt, Gerald Degenhart and Wolfgang Recheis for medical CT measurements at the Medical University of Innsbruck. Marcel Ortler and the Carinthian Institute of Lake Research (KIS) are thanked for technical and logistical support during fieldwork.

The authors thank Suzanne Bull and Katrina Kremer for the editorial handling of the manuscript, and Romain Vaucher, Liz Mahon and Sophie Hage for copyediting, layout and production. The authors also thank Renaldo Gastineau and an anonymous reviewer for their constructive reviews.

Authors contribution

Christoph Daxer: Data acquisition, formal analysis and interpretation, writing – original draft, writing – review & editing, visualization. Katleen Wils: Local seismic intensity calculation, writing – review & editing. Arne Ramisch: XRF Data analysis, writing – review & editing. Michael Strasser: data interpretation, writing – review & editing, funding acquisition. Jasper Moernaut: Data acquisition & interpretation, writing – original draft, writing – review & editing, project lead, funding acquisition. All authors have read the current manuscript and agreed to its publication.

Data availability

The seismic profiles, core scanning data as well as core photographs are available via Zenodo.org. https://doi.org/10.5281/zenodo.10785561.

Conflict of interest

The authors declare no conflict of interest.

References

Álvarez-Rubio, S., & Fäh, D. (2009). The BOXER method applied to the determination of earthquake parameters from macroseismic data - Verification of the calibration of historical earthquakes in the Earthquake Catalogue of Switzerland (ECOS2009). Internal Report of the Swiss Seismological Service, ETH Zürich, 1–24. http://www.seismo.ethz.ch/static/ecos-09/Appendix/Appendix_E.pdf

Anselmetti, F. S., Ariztegui, D., De Batist, M., Catalina Gebhardt, A., Haberzettl, T., Niessen, F., Ohlendorf, C., & Zolitschka, B. (2009). Environmental history of southern Patagonia unravelled by the seismic stratigraphy of Laguna Potrok Aike. Sedimentology, 56(4), 873–892. https://doi.org/10.1111/j.1365-3091.2008.01002.x

Archer, C., Noble, P., Rosen, M. R., Sagnotti, L., Florindo, F., Mensing, S., Piovesan, G., & Michetti, A. M. (2019). Lakes as paleoseismic records in a seismically-active, low-relief area (Rieti Basin, central Italy). Quaternary Science Reviews, 211, 186–207. https://doi.org/10.1016/j.quascirev.2019.03.004

Archer, D., Emerson, S., & Reimers, C. (1989). Dissolution of calcite in deep-sea sediments: pH and O_2 microelectrode results. Geochimica et Cosmochimica Acta, 53(11), 2831-2845. https://doi.org/10.1016/0016-7037(89)90161-0

Atanackov, J., Jamšek Rupnik, P., Jež, J., Celarc, B., Novak, M., Milanič, B., Markelj, A., Bavec, M., & Kastelic, V. (2021). Database of Active Faults in Slovenia: Compiling a New Active Fault Database at the Junction Between the Alps, the Dinarides and the Pannonian Basin Tectonic Domains. Frontiers in Earth Science, 9, 1–21. https://doi.org/10.3389/feart.2021.604388

Avşar, U., Hubert-Ferrari, A., De Batist, M., Lepoint, G., Schmidt, S., & Fagel, N. (2014). Seismically-triggered organic-rich layers in recent sediments from Göllüköy Lake (North Anatolian Fault, Turkey). Quaternary Science Reviews, 103, 67–80. https://doi.org/10.1016/j.quascirev.2014.08.020

Banjan, M., Christian, C., Pierre, S., Hervé, J., Manon, B., Francois, D., Anne-Lise, D., Jean-Philippe, J., Bernard, F., Emmanuel, M., Findling, N., Philippe, A., Julien, D., Vincent, B., Sylvain, C., & Erwan, M. (2023). Did the Younger Dryas to Holocene climate transition favour high seismicity rates in the north-western Alps? Sedimentology, 70(2), 538–568. https://doi.org/10.1111/sed.13050

Barfal, S. S., Das, M. M., Joshi, M., Joshi, R., Kumar, K., Kumar, D., & Rai, Y. K. (2022). Response of water springs towards an earthquake: A case study from Sikkim Himalaya. Journal of Applied Geophysics, 206, 104792. https://doi.org/10.1016/j.jappgeo.2022.104792

Baroň, I., Plan, L., Grasemann, B., Melichar, R., Mitrović-Woodell, I., Rowberry, M., & Scholz, D. (2022). Three large prehistoric earthquakes in the Eastern Alps evidenced by cave rupture and speleothem damage. Geomorphology, 408. https://doi.org/10.1016/j.geomorph.2022.108242

Baster, I., Girardclos, S., Pugin, A., & Wildi, W. (2003). High-resolution seismic stratigraphy of an Holocene lacustrine delta in western Lake Geneva (Switzerland). Eclogae Geologicae Helveticae, 96(Supplement 1), S11–S20. https://doi.org/0012-9402/03/01S011-10

Becker, A., Davenport, C. A., & Giardini, D. (2002). Palaeoseismicity studies on end-Pleistocene and Holocene lake deposits around Basle, Switzerland. Geophysical Journal International, 149(3), 659–678. https://doi.org/10.1046/j.1365-246X.2002.01678.x

Bigham, K. T., Rowden, A. A., Leduc, D., & Bowden, D. A. (2021). Review and syntheses: Impacts of turbidity flows on deep-sea benthic communities. Biogeosciences, 18(5), 1893–1908. https://doi.org/10.5194/bg-18-1893-2021

Blaauw, M., & Christen, J. A. (2011). Flexible paleoclimate age-depth models using an autoregressive gamma process. Bayesian Analysis, 6(3), 457–474. https://doi.org/10.1214/11-BA618

Blott, S. J., & Pye, K. (2001). GRADISTAT: a grain size distribution and statistics package for the analysis of unconsolidated sediments. Earth Surface Processes and Landforms, 26(11), 1237–1248. https://doi.org/10.1002/esp.261

Borasi, L., Cane, D., Fegerl, M., Fink, G., Fresner, R., Harum, T., Leis, A., Maffiotti, A., Provenzale, A., Reszler, C., Santner, G., Schulz, L., Siligardi, M., von Hardenberg, J., Wahl, B., Wolf, T., & Zennaro, B. (2013). Climate Change Impacts on Alpine Lakes. SILMAS Project-WP4: final guideline.

Bortenschlager, S. (1984). Beiträge zur Vegetationsgeschichte Tirols I. Inneres Ötztal und unteres Inntal. Berichte Des Naturwissenschaftlich-Medizinischen Vereins Innsbruck, 71, 19–56.

Brancelj, A., Žibrat, U., Mezek, T., Brancelj, I. R., & Dumont, H. J. (2012). Consecutive earthquakes temporarily restructured the zooplankton community in an Alpine Lake. Annales de Limnologie, 48(1), 113–123. https://doi.org/10.1051/limn/2012001

Brooks, G. R. (2018). Deglacial record of palaeoearthquakes interpreted from mass transport deposits at three lakes near Rouyn-Noranda, north-western Quebec, Canada. Sedimentology, 65(7), 2439–2467. https://doi.org/10.1111/sed.12473

Brückl, E., Behm, M., Decker, K., Grad, M., Guterch, A., Keller, G. R., & Thybo, H. (2010). Crustal structure and active tectonics in the Eastern Alps. Tectonics, 29(2). https://doi.org/10.1029/2009TC002491

Bundesministerium für Land- und Forstwirtschaft; Umwelt und Wasserwirtschaft. (2013). Hydrografisches Jahrbuch von Österreich 2013. https://wasser.umweltbundesamt.at/hydjb/historic/historic.xhtml#

Cai, W. J., Luther, G. W., Cornwell, J. C., & Giblin, A. E. (2010). Carbon cycling and the coupling between proton and electron transfer reactions in aquatic sediments in lake champlain. Aquatic Geochemistry, 16(3), 421–446. https://doi.org/10.1007/s10498-010-9097-9

Caracciolo, C. H., Camassi, R., & Castelli, V. (2015). I terremoto del 25 gennaio 1348 (Alpi orientali). Internal report, Istituto Nazionale di Geofisica e Vulcanologia, 12 pp. https://emidius.mi.ingv.it/ASMI/study/CARAL015

Caracciolo, C. H., Slejko, D., Camassi, R., & Castelli, V. (2021). The eastern alps earthquake of 25 january 1348: New insights from old sources. Bulletin of Geophysics and Oceanography, 62(3), 335–364. https://doi.org/10.4430/bgo00364

Croudace, I. W., & Rothwell, R. G. (2015). Micro-XRF Studies of Sediment Cores: Applications of a non-destructive tool for the environmental sciences. In Developments in Paleoenvironmental Research (Vol. 17). https://doi.org/10.1007/978-94-017-9849-5

Daxer, C., Huang, J.-J. S., Weginger, S., Hilbe, M., Strasser, M., & Moernaut, J. (2022a). Validation of seismic hazard curves using a calibrated 14 ka lacustrine record in the Eastern Alps, Austria. Scientific Reports, 12(1), 19943. https://doi.org/10.1038/s41598-022-24487-w

Daxer, C., Moernaut, J., Taylor, T., Haas, J. N., & Strasser, M. (2018). Late Glacial and Holocene sedimentary infill of Lake Mondsee (Eastern Alps, Austria) and historical rockfall activity revealed by reflection seismics and sediment core analysis. Austrian Journal of Earth Sciences, 111(1), 111–134. https://doi.org/10.17738/ajes.2018.0008

Daxer, C., Ortler, M., Fabbri, S. C., Hilbe, M., Hajdas, I., Dubois, N., Piechl, T., Hammerl, C., Strasser, M., & Moernaut, J. (2022b). High-resolution calibration of seismically-induced lacustrine deposits with historical earthquake data in the Eastern Alps (Carinthia, Austria). Quaternary Science Reviews, 284, 107497. https://doi.org/10.1016/j.quascirev.2022.107497

de Geer, G. (1912). Geochronologie der letzten 12000 Jahre. Geologische Rundschau, 3(7), 457–471. https://doi.org/10.1007/BF01802565

Draxler, I. (1977). Pollenanalytische Untersuchungen von Mooren zur spät- und postglazialen Vegetationsgeschichte im Einzugsgebiet der Traun. Jahrbuch Der Geologischen Bundesanstalt, 120(1), 131–163.

Eder, N., & Neubauer, F. (2000). On the edge of the extruding wedge: Neogene kinematics and geomorphology along the southern Niedere Tauern, Eastern Alps. Eclogae Geologicae Helvetiae, 93(1), 81–92.

Escoffier, N., Perolo, P., Many, G., Pasche, N. T., & Perga, M.-E. (2023). Fine-scale dynamics of calcite precipitation in a large hardwater lake. Science of The Total Environment, 864(August 2022), 160699. https://doi.org/10.1016/j.scitotenv.2022.160699

Fabbri, S. C., Buechi, M. W., Horstmeyer, H., Hilbe, M., Hübscher, C., Schmelzbach, C., Weiss, B., & Anselmetti, F.S. (2018). A subaquatic moraine complex in overdeepened Lake Thun (Switzerland) unravelling the deglaciation history of the Aare Glacier. Quaternary Science Reviews, 187, 62-79. https://doi.org/10.1016/j.quascirev.2018.03.010

Faccenna, C., Piromallo, C., Crespo-Blanc, A., Jolivet, L., & Rossetti, F. (2004). Lateral slab deformation and the origin of the western Mediterranean arcs. Tectonics, 23(1). https://doi.org/10.1029/2002TC001488

Fäh, D., Giardini, D., Kästli, P., Deichmann, N., Gisler, M., Schwarz-Zanetti, G., Alvarez-Rubio, S., Sellami, S., Edwards, B., & Allmann, B. (2011). ECOS-09 earthquake catalogue of Switzerland release 2011 report and database. Public catalogue, 17. 4. 2011. Swiss Seismological Service ETH Zurich. Risk, 1–42.

Folk, R. L., & Ward, W. C. (1957). Brazos River bar [Texas]; a study in the significance of grain size parameters. Journal of Sedimentary Research, 27(1), 3–26. https://doi.org/10.1306/74d70646-2b21-11d7-8648000102c1865d

Fritz, M., Herzschuh, U., Wetterich, S., Lantuit, H., De Pascale, G. P., Pollard, W. H., & Schirrmeister, L. (2012). Late glacial and Holocene sedimentation, vegetation, and climate history from easternmost Beringia (northern Yukon Territory, Canada). Quaternary Research (United States), 78(3), 549–560. https://doi.org/10.1016/j.yqres.2012.07.007

Gastineau, R., de Sigoyer, J., Sabatier, P., Fabbri, S. C., Anselmetti, F. S., Develle, A. L., Şahin, M., Gündüz, S., Niessen, F., & Gebhardt, A. C. (2021). Active Subaquatic Fault Segments in Lake Iznik Along the Middle Strand of the North Anatolian Fault, NW Turkey. Tectonics, 40(1), 1–22. https://doi.org/10.1029/2020TC006404

Girardclos, S., Schmidt, O. T., Sturm, M., Ariztegui, D., Pugin, A., & Anselmetti, F. S. (2007). The 1996 AD delta collapse and large turbidite in Lake Brienz. Marine Geology, 241(1–4), 137–154. https://doi.org/10.1016/j.margeo.2007.03.011

Gleirscher, P. (1996). Spätkeltische und frührömische Funde im Bereich der Gracarca am Klopeiner See (Unterkärnten). Arheološki Vestnik, 47, 229–238.

Gleirscher, P. (2009). Gräber keltischer Schwertkrieger vom Fuße der Gracarca (Kärnten). In Protohistoire Européenne (Issue 11).

Grünthal, G., Wahlström, R., & Stromeyer, D. (2013). The SHARE European Earthquake Catalogue (SHEEC) for the time period 1900-2006 and its comparison to the European-Mediterranean Earthquake Catalogue (EMEC). Journal of Seismology, 17(4), 1339–1344. https://doi.org/10.1007/s10950-013-9379-y

Gälman, V., Rydberg, J., Shchukarev, A., Sjöberg, S., Martínez-Cortizas, A., Bindler, R., & Renberg, I. (2009). The role of iron and sulfur in the visual appearance of lake sediment varves. Journal of Paleolimnology, 42, 141-153. https://doi.org/10.1007/s10933-008-9267-6

Hammerl, C. (1994). The earthquake of January 25th, 1348, discussion of sources. Historical Investigation of European Earthquakes. Materials of the CEC Project "Review of Historical Seismicity in Europe," 2, 225–240.

Hammerl, C. (2017). Historical earthquake research in Austria. Geoscience Letters, 4(1), 7. https://doi.org/10.1186/s40562-017-0073-8

Harrison, B. K., Myrbo, A., Flood, B. E., & Bailey, J. V. (2018). Abrupt burial imparts persistent changes to the bacterial diversity of turbidite-associated sediment profiles. Geobiology, 16(2), 190–202. https://doi.org/10.1111/gbi.12271

Heerema, C. J., Talling, P. J., Cartigny, M. J., Paull, C. K., Bailey, L., Simmons, S. M., Parsons, D. R., Clare, M. A., Gwiazda, R., Lundsten, E., Anderson, K., Maier, K. L., Xu, J. P., Sumner, E. J., Rosenberger, K., Gales, J., McGann, M., Carter, L., & Pope, E. (2020). What determines the downstream evolution of turbidity currents? Earth and Planetary Science Letters, 532. https://doi.org/10.1016/j.epsl.2019.116023

Hernández-Almeida, I., Grosjean, M., Tylmann, W., & Bonk, A. (2015). Chrysophyte cyst-inferred variability of warm season lake water chemistry and climate in northern Poland: training set and downcore reconstruction. Journal of Paleolimnology, 53(1), 123–138. https://doi.org/10.1007/s10933-014-9812-4

Hilbe, M., & Anselmetti, F. S. (2014). Signatures of slope failures and river-delta collapses in a perialpine lake (Lake Lucerne, Switzerland). Sedimentology, 61(7), 1883–1907. https://doi.org/10.1111/sed.12120

Howarth, J. D., Barth, N. C., Fitzsimons, S. J., Richards-Dinger, K., Clark, K. J., Biasi, G. P., Cochran, U. A., Langridge, R. M., Berryman, K. R., & Sutherland, R. (2021). Spatiotemporal clustering of great earthquakes on a transform fault controlled by geometry. Nature Geoscience, 14(5), 314–320. https://doi.org/10.1038/s41561-021-00721-4

Howarth, J. D., Orpin, A. R., Kaneko, Y., Strachan, L. J., Nodder, S. D., Mountjoy, J. J., Barnes, P. M., Bostock, H. C., Holden, C., Jones, K., & Cağatay, M. N. (2016). Calibrating the marine turbidite palaeoseismometer using the 2016 Kaikōura earthquake. Nature Geoscience, 14, 167–167. https://doi.org/10.1038/s41561-021-00692-6

Huber, K., Weckström, K., Drescher-Schneider, R., Knoll, J., Schmidt, J., & Schmidt, R. (2010). Climate changes during the last glacial termination inferred from diatom-based temperatures and pollen in a sediment core from Längsee (Austria). Journal of Paleolimnology, 43(1), 131–147. https://doi.org/10.1007/s10933-009-9322-y

Jackson, D. D., & Anderson, D. L. (1970). Physical mechanisms of seismic-wave attenuation. Reviews of Geophysics, 8(1), 1. https://doi.org/10.1029/RG008i001p00001

Jakobsson, M., Björck, S., O'Regan, M., Flodén, T., Greenwood, S. L., Swärd, H., Lif, A., Ampel, L., Koyi, H., & Skelton, A. (2014). Major earthquake at the Pleistocene-Holocene transition in Lake Vättern, Southern Sweden. Geology, 42(5), 379–382. https://doi.org/10.1130/G35499.1

Kahler, F. (1962). Geologische Karte der Umgebung von Klagenfurt 1:50000. Geologische Bundesanstalt.

Kärntner Institut für Seenforschung (2021). Seenbericht Klopeiner See. Kärntner Seen - Bericht. https://kis.ktn.gv.at/seen/kaerntner-seen?seeid=19&berichtjahr=2021

Kastelic, V., Vrabec, M., Cunningham, D., & Gosar, A. (2008). Neo-Alpine structural evolution and present-day tectonic activity of the eastern Southern Alps: The case of the Ravne Fault, NW Slovenia. Journal of Structural Geology, 30(8), 963–975. https://doi.org/10.1016/j.jsg.2008.03.009

Khan, H., Laas, A., Marcé, R., Sepp, M., & Obrador, B. (2021). Eutrophication and geochemistry drive pelagic calcite precipitation in lakes. Water (Switzerland), 13(5), 1–15. https://doi.org/10.3390/w13050597

Kienel, U., Dulski, P., Ott, F., Lorenz, S., & Brauer, A. (2013). Recently induced anoxia leading to the preservation of seasonal laminae in two NE-German lakes. Journal of Paleolimnology, 50(4), 535–544. https://doi.org/10.1007/s10933-013-9745-3

Kremer, K., Gassner-Stamm, G., Grolimund, R., Wirth, S. B., Strasser, M., & Fäh, D. (2020). A database of potential paleoseismic evidence in Switzerland. Journal of Seismology, 24(2), 247–262. https://doi.org/10.1007/s10950-020-09908-5

Kremer, K., Simpson, G., & Girardclos, S. (2012). Giant Lake Geneva tsunami in AD 563. Nature Geoscience, 5(11), 756–757. https://doi.org/10.1038/ngeo1618

Kremer, K., Wirth, S. B., Reusch, A., Fäh, D., Bellwald, B., Anselmetti, F. S., Girardclos, S., & Strasser, M. (2017). Lake-sediment based paleoseismology: Limitations and perspectives from the Swiss Alps. Quaternary Science Reviews, 168, 1–18. https://doi.org/10.1016/j.quascirev.2017.04.026

Landgraf, A., KüBler, S., Hintersberger, E., & Stein, S. (2017). Active tectonics, earthquakes and palaeoseismicity in slowly deforming continents. Geological Society Special Publication, 432(1), 1–12. https://doi.org/10.1144/SP432.13

Lenhardt, W. A. (2007). Earthquake-Triggered Landslides in Austria-Dobratsch Revisited. Jahrbuch Der Geologischen Bundesanstalt, 147(1+2), 193–199. www.geologie.ac.at

Lenhardt, W. A., Freudenthaler, C., Lippitsch, R., & Fiegweil, E. (2007). Focal-depth distributions in the Austrian Eastern Alps based on macroseismic data. Austrian Journal of Earth Sciences, 100, 66–79.

Manga, M., & Wang, C.-Y. (2015). Earthquake Hydrology. In Treatise on Geophysics (Vol. 4, pp. 305–328). Elsevier. https://doi.org/10.1016/B978-0-444-53802-4.00082-8

Messiner, H., & Windisch, H. (2008). Der Klopeiner See – Eigenschaften und Dynamik. Ein Beitrag zur Kenntnis dieses Sees. Carinthia II, 198(118), 501–542.

Michetti, A. M., Esposito, E., Guerrieri, L., Porfido, S., Serva, L., Tatevossian, R., Vittori, E., Audemard, F. A., Azuma, T., Clague, J., Comerci, V., Gürpinar, A., McCalpin, J., Mohammadioun, B., Mörner, N. A., Ota, Y., & Roghozin, E. (2007). Environmental Seismic Intensity Scale - ESI 2007. In E. Vittori & L. Guerrieri (Eds.), Memorie Descrittive della Carta Geologica d'Italia: Vol. LXXIV (Issue May 2014, pp. 7–54). Servizio Geologico d'Italia.

Moernaut, J. (2020). Time-dependent recurrence of strong earthquake shaking near plate boundaries: A lake sediment perspective. Earth-Science Reviews, 210, 103344. https://doi.org/10.1016/j.earscirev.2020.103344

Moernaut, J., Daele, M. Van, Heirman, K., Fontijn, K., Strasser, M., Pino, M., Urrutia, R., & De Batist, M. (2014). Lacustrine turbidites as a tool for quantitative earthquake reconstruction: New evidence for a variable rupture mode in south central Chile. Journal of Geophysical Research: Solid Earth, 119(3), 1607–1633. https://doi.org/10.1002/2013JB010738

Moernaut, J., De Batist, M., Charlet, F., Heirman, K., Chapron, E., Pino, M., Brümmer, R., & Urrutia, R. (2007). Giant earthquakes in South-Central Chile revealed by Holocene mass-wasting events in Lake Puyehue. Sedimentary Geology, 195(3–4), 239–256. https://doi.org/10.1016/j.sedgeo.2006.08.005

Moernaut, J., Van Daele, M., Strasser, M., Clare, M. A., Heirman, K., Viel, M., Cardenas, J., Kilian, R., Ladrón de Guevara, B., Pino, M., Urrutia, R., & De Batist, M. (2017). Lacustrine turbidites produced by surficial slope sediment remobilization: A mechanism for continuous and sensitive turbidite paleoseismic records. Marine Geology, 384, 159–176. https://doi.org/10.1016/j.margeo.2015.10.009

Molenaar, A., Van Daele, M., Huang, J. J. S., Strasser, M., De Batist, M., Pino, M., Urrutia, R., & Moernaut, J. (2022). Disentangling factors controlling earthquake-triggered soft-sediment deformation in lakes. Sedimentary Geology, 438, 106200. https://doi.org/10.1016/j.sedgeo.2022.106200

Molenaar, A., Van Daele, M., Vandorpe, T., Degenhart, G., De Batist, M., Urrutia, R., Pino, M., Strasser, M., & Moernaut, J. (2021). What controls the remobilization and deformation of surficial sediment by seismic shaking? Linking lacustrine slope stratigraphy to great earthquakes in South–Central Chile. Sedimentology, 68(6), 2365–2396. https://doi.org/10.1111/sed.12856

Molina, J. M., Alfaro, P., Moretti, M., & Soria, J. M. (1998). Soft-sediment deformation structures induced by cyclic stress of storm waves in tempestites (Miocene, Guadalquivir Basin, Spain). Terra Nova, 10(3), 145–150. https://doi.org/10.1046/j.1365-3121.1998.00183.x

Monecke, K., Anselmetti, F. S., Becker, A., Schnellmann, M., Sturm, M., & Giardini, D. (2006). Earthquake-induced deformation structures in lake deposits: A Late Pleistocene to Holocene paleoseismic record for Central Switzerland. Eclogae Geologicae Helvetiae, 99(3), 343–362. https://doi.org/10.1007/s00015-006-1193-x

Monecke, K., Anselmetti, F. S., Becker, A., Sturm, M., & Giardini, D. (2004). The record of historic earthquakes in lake sediments of Central Switzerland. Tectonophysics, 394(1–2), 21–40. https://doi.org/10.1016/j.tecto.2004.07.053

Monegato, G., Ravazzi, C., Donegana, M., Pini, R., Calderoni, G., & Wick, L. (2007). Evidence of a two-fold glacial advance during the last glacial maximum in the Tagliamento end moraine system (eastern Alps). Quaternary Research, 68(2), 284–302. https://doi.org/10.1016/j.yqres.2007.07.002

Moser, M. (2020). GEOFAST 1:50.000 – Zusammenstellung ausgewählter Archivunterlagen der Geologischen Bundesanstalt, Blatt 204 Völkermarkt. Geologische Bundesanstalt.

Munsell. (2010). Munsell soil color charts : with genuine Munsell color chips. 2009 year revised. Grand Rapids, MI : Munsell Color, 2010. https://search.library.wisc.edu/catalog/9910109259802121

Müller, B., Wang, Y., Dittrich, M., & Wehrli, B. (2003). Influence of organic carbon decomposition on calcite dissolution in surficial sediments of a freshwater lake. Water Research, 37(18), 4524-4532, https://doi.org/10.1016/S0043-1354(03)00381-6

Müller, B., Wang, Y., Wehrli, B. (2006). Cycling of calcite in hard water lakes of different trophic states. Limnology and Oceanography, 51, 1678-1688, 10.4319/lo.2006.51.4.1678

Ndiaye, M., Clerc, N., Gorin, G., Girardclos, S., & Fiore, J. (2014). Lake Neuchâtel (Switzerland) seismic stratigraphic record points to the simultaneous Würmian deglaciation of the Rhône Glacier and Jura Ice Cap. Quaternary Science Reviews, 85, 1–19. https://doi.org/10.1016/j.quascirev.2013.11.017

Nemes, F., Neubauer, F., Cloetingh, S., & Genser, J. (1997). The Klagenfurt Basin in the Eastern Alps: An intra-orogenic decoupled flexural basin? Tectonophysics, 282(1–4), 189–203. https://doi.org/10.1016/S0040-1951(97)00219-9

Ohlendorf, C., & Sturm, M. (2018). Precipitation and Dissolution of Calcite in a Swiss High Alpine Lake. Arctic, Antarctic, and Alpine Research, 33, 410-417. https://doi.org/10.1080/15230430.2001.12003449

Ojala, A. E. K., Kosonen, E., Weckström, J., Korkonen, S., & Korhola, A. (2013). Seasonal formation of clastic-biogenic varves: the potential for palaeoenvironmental interpretations. GFF, 135(3-4), 237-247. https://doi.org/10.1080/11035897.2013.801925

Ojala, A. E. K., Mattila, J., Hämäläinen, J., & Sutinen, R. (2019). Lake sediment evidence of paleoseismicity: Timing and spatial occurrence of late- and postglacial earthquakes in Finland. Tectonophysics, 771, 228227. https://doi.org/10.1016/j.tecto.2019.228227

Oswald, P., Strasser, M., Hammerl, C., & Moernaut, J. (2021). Seismic control of large prehistoric rockslides in the Eastern Alps. Nature Communications, 12(1), 1059. https://doi.org/10.1038/s41467-021-21327-9

Oswald, P., Strasser, M., Skapski, J., Moernaut, J., & Oswald, C. P. (2022). Magnitude and source area estimations of severe prehistoric earthquakes in the western Austrian Alps. Natural Hazards and Earth System Sciences, 22, 2057–2079, https://doi.org/10.5194/nhess-22-2057-2022

Owen, G. (2003). Load structures: Gravity-driven sediment mobilization in the shallow subsurface. Geological Society, London, Special Publications, 216, 21–34. https://doi.org/10.1144/GSL.SP.2003.216.01.03

Oxburgh, R., & Broecker, W. S. (1993). Pacific carbonate dissolution revisited. Palaeogeography, Palaeoclimatology, Palaeoecology, 103(1-2), 31-40. https://doi.org/10.1016/0031-0182(93)90049-O

Palmer, A. P., Bendle, J. M., MacLeod, A., Rose, J., & Thorndycraft, V. R. (2019). The micromorphology of glaciolacustrine varve sediments and their use for reconstructing palaeoglaciological and palaeoenvironmental change. Quaternary Science Reviews, 226, 105964. https://doi.org/10.1016/j.quascirev.2019.105964

Polonia, A., Albertazzi, S., Bellucci, L. G., Bonetti, C., Bonetti, J., Giorgetti, G., Giuliani, S., Correa, M. L., Mayr, C., Peruzza, L., Stanghellini, G., & Gasperini, L. (2021). Decoding a complex record of anthropogenic and natural impacts in the Lake of Cavazzo sediments, NE Italy. Science of the Total Environment, 787, 147659. https://doi.org/10.1016/j.scitotenv.2021.147659

Praet, N. (2020). Towards the construction of a lacustrine paleoseismic record in south-central Alaska : a trembling tale of landslides and turbidites. PhD Thesis, Ghent University. http://hdl.handle.net/1854/LU-8681726

Praet, N., Moernaut, J., Van Daele, M., Boes, E., Haeussler, P. J., Strupler, M., Schmidt, S., Loso, M. G., & De Batist, M. (2017). Paleoseismic potential of sublacustrine landslide records in a high-seismicity setting (south-central Alaska). Marine Geology, 384, 103–119. https://doi.org/10.1016/j.margeo.2016.05.004

Praet, N., Van Daele, M., Collart, T., Moernaut, J., Vandekerkhove, E., Kempf, P., Haeussler, P. J., & De Batist, M. (2020). Turbidite stratigraphy in proglacial lakes: Deciphering trigger mechanisms using a statistical approach. Sedimentology, 67(5), 2332–2359. https://doi.org/10.1111/sed.12703

Praet, N., Van Daele, M., Moernaut, J., Mestdagh, T., Vandorpe, T., Jensen, B. J. L., Witter, R. C., Haeussler, P. J., & De Batist, M. (2022). Unravelling a 2300 year long sedimentary record of megathrust and intraslab earthquakes in proglacial Skilak Lake, south-central Alaska. Sedimentology, 69(5), 2151–2180. https://doi.org/10.1111/sed.12986

Rapuc, W., Arnaud, F., Sabatier, P., Anselmetti, F. S., Piccin, A., Peruzza, L., Bastien, A., Augustin, L., Régnier, E., Gaillardet, J., & Von Grafenstein, U. (2022). Instant sedimentation in a deep Alpine lake (Iseo, Italy) controlled by climate, human and geodynamic forcing. Sedimentology, 69(4), 1816–1840. https://doi.org/10.1111/sed.12972

Rapuc, W., Sabatier, P., Andrič, M., Crouzet, C., Arnaud, F., Chapron, E., Šmuc, A., Develle, A. L., Wilhelm, B., Demory, F., Reyss, J. L., Régnier, E., Daut, G., & Von Grafenstein, U. (2018). 6600 years of earthquake record in the Julian Alps (Lake Bohinj, Slovenia). Sedimentology, 65(5), 1777–1799. https://doi.org/10.1111/sed.12446

Ratschbacher, L., Frisch, W., Linzer, H.-G., & Merle, O. (1991). Lateral extrusion in the eastern Alps, Part 2: Structural analysis. Tectonics, 10(2), 257–271. https://doi.org/10.1029/90TC02623

Reichmann, M., Fresner, R., & Schulz, L. (2014). Meromixis an Kärntner Seen. Denisia, 33, 129–133.

Reimer, P. J., Austin, W. E. N., Bard, E., Bayliss, A., Blackwell, P. G., Bronk Ramsey, C., Butzin, M., Cheng, H., Edwards, R. L., Friedrich, M., Grootes, P. M., Guilderson, T. P., Hajdas, I., Heaton, T. J., Hogg, A. G., Hughen, K. A., Kromer, B., Manning, S. W., Muscheler, R., … Talamo, S. (2020). The IntCal20 Northern Hemisphere Radiocarbon Age Calibration Curve (0-55 cal kBP). Radiocarbon, 62(4), 725–757. https://doi.org/10.1017/RDC.2020.41

Reinecker, J., & Lenhardt, W. A. (1999). Present-day stress field and deformation in eastern Austria. International Journal of Earth Sciences, 88(3), 532–550. https://doi.org/10.1007/s005310050283

Reitner, J. M. (2007). Glacial dynamics at the beginning of Termination I in the Eastern Alps and their stratigraphic implications. Quaternary International, 164–165, 64–84. https://doi.org/10.1016/j.quaint.2006.12.016

Reusch, A., Loher, M., Bouffard, D., Moernaut, J., Hellmich, F., Anselmetti, F. S., Bernasconi, S. M., Hilbe, M., Kopf, A., Lilley, M. D., Meinecke, G., & Strasser, M. (2015). Giant lacustrine pockmarks with subaqueous groundwater discharge and subsurface sediment mobilization. Geophysical Research Letters, 42(9), 3465–3473. https://doi.org/10.1002/2015GL064179

Reusch, A., Moernaut, J., Anselmetti, F. S., & Strasser, M. (2016). Sediment mobilization deposits from episodic subsurface fluid flow-A new tool to reveal long-term earthquake records? Geology, 44(4), 243–246. https://doi.org/10.1130/G37410.1

Ridge, J. C., Balco, G., Bayless, R. L., Beck, C. C., Carter, L. B., Dean, J. L., Voytek, E. B., & Wei, J. H. (2012). The new north american varve chronology: A precise record of southeastern laurentide ice sheet deglaciation and climate, 18.2-12.5 kyr BP, and correlations with greenland ice core records. American Journal of Science, 312(7), 685–722. https://doi.org/10.2475/07.2012.01

Roberts, S. J., McCulloch, R. D., Emmings, J. F., Davies, S. J., Van Nieuwenhuyze, W., Sterken, M., Heirman, K., Van Wichelen, J., Diaz, C., Van de Vyver, E., Whittle, A., Vyverman, W., Hodgson, D. A., & Verleyen, E. (2022). Late Glacial and Holocene Palaeolake History of the Última Esperanza Region of Southern Patagonia. Frontiers in Earth Science, 10, 1–32. https://doi.org/10.3389/feart.2022.813396

Rovida, A., Antonucci, A., & Locati, M. (2022). The European Preinstrumental Earthquake Catalogue EPICA, the 1000-1899 catalogue for the European Seismic Hazard Model 2020. Earth System Science Data, 14(12), 5213–5231. https://doi.org/10.5194/essd-14-5213-2022

Sammartini, M., Moernaut, J., Anselmetti, F. S., Hilbe, M., Lindhorst, K., Praet, N., & Strasser, M. (2019). An atlas of mass-transport deposits in lakes. Submarine Landslides: Subaqueous Mass Transport Deposits from Outcrops to Seismic Profiles, 201–226. https://doi.org/10.1002/9781119500513.ch13

Sánchez, L., Völksen, C., Sokolov, A., Arenz, H., & Seitz, F. (2018). Present-day surface deformation of the Alpine region inferred from geodetic techniques. Earth System Science Data, 10(3), 1503–1526. https://doi.org/10.5194/essd-10-1503-2018

Sbarra, P., Burrato, P., De Rubeis, V., Tosi, P., Valensise, G., Vallone, R., & Vannoli, P. (2023). Inferring the depth and magnitude of pre-instrumental earthquakes from intensity attenuation curves. Natural Hazards and Earth System Sciences, 23(3), 1007–1028. https://doi.org/10.5194/nhess-23-1007-2023

Schindelin, J., Arganda-Carreras, I., Frise, E., Kaynig, V., Longair, M., Pietzsch, T., Preibisch, S., Rueden, C., Saalfeld, S., Schmid, B., Tinevez, J.-Y., White, D. J., Hartenstein, V., Eliceiri, K., Tomancak, P., & Cardona, A. (2012). Fiji: an open-source platform for biological-image analysis. Nature Methods, 9(7), 676–682. https://doi.org/10.1038/nmeth.2019

Schmid, S. M., Fügenschuh, B., Kissling, E., & Schuster, R. (2004). Tectonic map and overall architecture of the Alpine orogen. Eclogae Geologicae Helvetiae, 97(1), 93–117. https://doi.org/10.1007/s00015-004-1113-x

Schmidt, R., Weckström, K., Lauterbach, S., Tessadri, R., & Huber, K. (2012). North Atlantic climate impact on early late-glacial climate oscillations in the south-eastern Alps inferred from a multi-proxy lake sediment record. Journal of Quaternary Science, 27(1), 40–50. https://doi.org/10.1002/jqs.1505

Schmidt, R., Wunsam, S., Brosch, U., Fott, J., Lami, A., Löffler, H., Marchetto, A., Müller, H. W., Pražáková, M., & Schwaighofer, B. (1998). Late and post-glacial history of meromictic Langsee (Austria), in respect to climate change and anthropogenic impact. Aquatic Sciences, 60(1), 56–88. https://doi.org/10.1007/s000270050026

Schnellmann, M., Anselmetti, F. S., Giardini, D., & Mckenzie, J. A. (2006). 15,000 Years of mass-movement history in Lake Lucerne: Implications for seismic and tsunami hazards. Eclogae Geologicae Helvetiae, 99(3), 409–428. https://doi.org/10.1007/s00015-006-1196-7

Schnellmann, M., Anselmetti, F. S., Giardini, D., McKenzie, J. A., & Ward, S. N. (2002). Prehistoric earthquake history revealed by lacustrine slump deposits. Geology, 30(12), 1131. https://doi.org/10.1130/0091-7613(2002)030<1131:PEHRBL>2.0.CO;2

Schnurrenberger, D., Russel, J., & Kelts, K. (2003). Classification of lacustrine sediments based on sedimentary components. Journal of Paleolimnology, 29(2), 141–154. https://doi.org/10.1023/A:1023270324800

Seguinot, J., Ivy-Ochs, S., Jouvet, G., Huss, M., Funk, M., & Preusser, F. (2018). Modelling last glacial cycle ice dynamics in the Alps. The Cryosphere, 12(10), 3265–3285. https://doi.org/10.5194/tc-12-3265-2018

Shchukarev, A., Gälman, V., Rydberg, J., Sjöberg, S., & Renberg, I. (2008). Speciation of iron and sulphur in seasonal layers of varved lake sediment: an XPS study. Surface and Interface Analysis, 40(3-4), 354-357. https://doi.org/10.1002/sia.2704

Sims, J. D. (1973). Earthquake-Induced Structures in Sediments of Van Norman Lake, San Fernando, California. Science, 182(4108), 161–163. https://doi.org/10.1126/science.182.4108.161

Song, D., Che, A., Zhu, R., & Ge, X. (2019). Natural Frequency Characteristics of Rock Masses Containing a Complex Geological Structure and Their Effects on the Dynamic Stability of Slopes. Rock Mechanics and Rock Engineering, 52(11), 4457–4473. https://doi.org/10.1007/s00603-019-01885-7

Stein, S., & Liu, M. (2009). Long aftershock sequences within continents and implications for earthquake hazard assessment. Nature, 462(7269), 87–89. https://doi.org/10.1038/nature08502

Stiny, V. J. (1934). Zur Kenntnis der Hochfläche von Rückersdorf (Kärnten). Jahrbuch Der Geologischen Bundesanstalt, 546.

Strasser, M., Anselmetti, F. S., Fäh, D., Giardini, D., & Schnellmann, M. (2006). Magnitudes and source areas of large

prehistoric northern Alpine earthquakes revealed by slope failures in lakes. Geology, 34(12), 1005. https://doi.org/10.1130/G22784A.1

Strasser, M., Monecke, K., Schnellmann, M., & Anselmetti, F. S. (2013). Lake sediments as natural seismographs: A compiled record of Late Quaternary earthquakes in Central Switzerland and its implication for Alpine deformation. Sedimentology, 60(1), 319–341. https://doi.org/10.1111/sed.12003

Stucchi, M., Rovida, A., Gomez Capera, A. A., Alexandre, P., Camelbeeck, T., Demircioglu, M. B., Gasperini, P., Kouskouna, V., Musson, R. M. W., Radulian, M., Sesetyan, K., Vilanova, S., Baumont, D., Bungum, H., Fäh, D., Lenhardt, W., Makropoulos, K., Martinez Solares, J. M., Scotti, O., … Giardini, D. (2013). The SHARE European Earthquake Catalogue (SHEEC) 1000–1899. Journal of Seismology, 17(2), 523–544. https://doi.org/10.1007/s10950-012-9335-2

Sulpis, O., Lix, C., Mucci, A., & Boudreau, B. (2017). Calcite dissolution kinetics at the sediment-water interface in natural seawater. Marine Chemistry, 195, 70-83. https://doi.org/10.1016/j.marchem.2017.06.005

Szczerba, A., Pla-Rabes, S., & Tylmann, W. (2023). Control of diatom and chrysophyte cyst dynamics by a meteorologically driven mixing regime in eutrophic Lake Żabińskie, northern Poland. Freshwater Biology, March, 1–15. https://doi.org/10.1111/fwb.14144

Tiberi, L., Costa, G., & Suhadolc, P. (2014). Source parameter estimates for some historical earthquakes in the south-eastern Alps using ground shaking scenarios. Bollettino Di Geofisica Teorica Ed Applicata, 55(3), 641–664. https://doi.org/10.4430/bgta0121

Van Daele, M., Araya-Cornejo, C., Pille, T., Vanneste, K., Moernaut, J., Schmidt, S., Kempf, P., Meyer, I., & Cisternas, M. (2019). Distinguishing intraplate from megathrust earthquakes using lacustrine turbidites. Geology, 47(2), 127–130. https://doi.org/10.1130/G45662.1

van Husen, D. (1987). Die Ostalpen in den Eiszeiten. Geologische Bundesanstalt. 24 pp.

van Husen, D. (2011). Quaternary Glaciations in Austria. In Developments in Quaternary Science (1st ed., Vol. 15, pp. 15–28). Elsevier Inc. https://doi.org/10.1016/B978-0-444-53447-7.00002-7

van Loon, A. J., Pisarska-Jamroży, M., Nartišs, M., Krievāns, M., & Soms, J. (2016). Seismites resulting from high-frequency, high-magnitude earthquakes in Latvia caused by Late Glacial glacio-isostatic uplift. Journal of Palaeogeography, 5(4), 363–380. https://doi.org/10.1016/j.jop.2016.05.002

Van Rensbergen, P., De Batist, M., Beck, C., & Manalt, F. (1998). High-resolution seismic stratigraphy of late quaternary fill of Lake Annecy (northwestern Alps): evolution from glacial to interglacial sedimentary processes. Sedimentary Geology, 117(1-2), 71-96. https://doi.org/10.1016/S0037-0738(97)00123-1

Vandekerkhove, E., Van Daele, M., Praet, N., Cnudde, V., Haeussler, P. J., & De Batist, M. (2020). Flood-triggered versus earthquake-triggered turbidites: A sedimentological study in clastic lake sediments (Eklutna Lake, Alaska). Sedimentology, 67(1), 364–389. https://doi.org/10.1111/sed.12646

Vanneste, K., Wils, K., & Van Daele, M. (2018). Probabilistic Evaluation of Fault Sources Based on Paleoseismic Evidence From Mass-Transport Deposits: The Example of Aysén Fjord, Chile. Journal of Geophysical Research: Solid Earth, 123(11), 9842–9865. https://doi.org/10.1029/2018JB016289

Wachniew, P., & Różański, K. (1997). Carbon budget of a mid-latitude, groundwater-controlled lake: Isotopic evidence for the importance of dissolved inorganic carbon recycling. Geochimica et Cosmochimica Acta, 61(12), 2453-2465. https://doi.org/10.1016/S0016-7037(97)00089-6

Wang, C. Y., & Manga, M. (2015). New streams and springs after the 2014 Mw6.0 South Napa earthquake. Nature Communications, 6, 6–11. https://doi.org/10.1038/ncomms8597

Ward, J. H. (1963). Hierarchical Grouping to Optimize an Objective Function. Journal of the American Statistical Association, 58(301), 236–244. https://doi.org/10.1080/01621459.1963.10500845

Weginger, S., Jia, Y., Papi-Isaba, M., Lenhardt, W., & Hausmann, H. (2019). Entwicklung einer regionalen Erdbebengefährdungskarte für Österreich. D-A-CH Tagungsband, 16, 27–34.

Wehr, J. D., & Sheath, R. (2003). Freshwater Habitats of Algae. Freshwater Algae of North America: Ecology and Classification, 11-57. https://doi.org/10.1016/B978-012741550-5/50003-9

Weltje, G. J., Bloemsma, M. R., Tjallingii, R., Heslop, D., Röhl, U., & Croudace, I. W. (2015). Prediction of Geochemical Composition from XRF Core Scanner Data: A New Multivariate Approach Including Automatic Selection of Calibration Samples and Quantification of Uncertainties. In: Croudace, I., Rothwell, R. (eds) Micro-XRF Studies of Sediment Cores. Developments in Paleoenvironmental Research, vol 17. Springer, Dordrecht. https://doi.org/10.1007/978-94-017-9849-5_21

Wilhelm, B., Nomade, J., Crouzet, C., Litty, C., Sabatier, P., Belle, S., Rolland, Y., Revel, M., Courboulex, F., Arnaud, F., & Anselmetti, F. S. (2016). Quantified sensitivity of small lake sediments to record historic earthquakes: Implications for paleoseismology. Journal of Geophysical Research: Earth Surface, 121(1), 2–16. https://doi.org/10.1002/2015JF003644

Wils, K., Van Daele, M., Kissel, C., Moernaut, J., Schmidt, S., Siani, G., & Lastras, G. (2020). Seismo-Turbidites in Aysén Fjord (Southern Chile) Reveal a Complex Pattern of Rupture Modes Along the 1960 Megathrust Earthquake Segment. Journal of Geophysical Research: Solid Earth, 125(9), 1–23. https://doi.org/10.1029/2020JB019405

ZAMG. (2021). AEC - Austrian Earthquake Catalogue. Seismological Service of the Zentralanstalt für Meteorologie und Geodynamik (ZAMG).

Zolitschka, B., Francus, P., Ojala, A. E. K., & Schimmelmann, A. (2015). Varves in lake sediments - a review. Quaternary Science Reviews, 117, 1–41. https://doi.org/10.1016/j.quascirev.2015.03.019

How to cite: Daxer, C., Wils, K., Ramisch, A., Strasser, M., & Moernaut, J. (2024). Contrasting sedimentary and long-lasting geochemical imprints of seismic shaking in a small, groundwater-fed lake basin (Klopeiner See, Eastern European Alps). Sedimentologika, 2(1), 1-27. https://doi.org/10.57035/journals/sdk.2024.e21.1296